Exclusive hadronic B decays to charm and charmonium final states

ALAM, M.; et al.

M. THULASIDAS
Singapore Management University, manojt@smu.edu.sg

Citation

1

ARTICLES

Exclusive hadronic B decays to charm and charmonium final states

M.S. Alam,[1] I.J. Kim,[1] B. Nemati,[1] J.J. O'Neill,[1] H. Severini,[1] C.R. Sun,[1] M.M. Zoeller,[1] G. Crawford,[2]
C. M. Daubenmier,[2] R. Fulton,[2] D. Fujino,[2] K.K. Gan,[2] K. Honscheid,[2] H. Kagan,[2] R. Kass,[2] J. Lee,[2] R. Malchow,[2]
F. Morrow,[2] Y. Skovpen,[2,*] M. Sung,[2] C. White,[2] F. Butler,[3] X. Fu,[3] G. Kalbfleisch,[3] W.R. Ross,[3] P. Skubic,[3]
J. Snow,[3] P.L. Wang,[3] M. Wood,[3] D.N. Brown,[4] J. Fast, [4] R.L. McIlwain,[4] T. Miao,[4] D.H. Miller,[4] M. Modesitt,[4]
D. Payne,[4] E.I. Shibata,[4] I.P.J. Shipsey,[4] P.N. Wang,[4] M. Battle,[5] J. Ernst,[5] Y. Kwon,[5] S. Roberts,[5]
E.H. Thorndike,[5] C.H. Wang,[5] J. Dominick,[6] M. Lambrecht,[6] S. Sanghera,[6] V. Shelkov,[6] T. Skwarnicki,[6]
R. Stroynowski,[6] I. Volobouev,[6] G. Wei,[6] P. Zadorozhny,[6] M. Artuso,[7] M. Goldberg,[7] D. He,[7] N. Horwitz,[7]
R. Kennett,[7] R. Mountain,[7] G.C. Moneti,[7] F. Muheim,[7] Y. Mukhin,[7] S. Playfer,[7] Y. Rozen,[7] S. Stone,[7]
M. Thulasidas,[7] G. Vasseur,[7] G. Zhu,[7] J. Bartelt,[8] S.E. Csorna,[8] Z. Egyed,[8] V. Jain,[8] K. Kinoshita,[9]
K.W. Edwards,[10] M. Ogg,[10] D.I. Britton,[11] E.R.F. Hyatt,[11] D.B. MacFarlane,[11] P.M. Patel,[11] D.S. Akerib,[12]
B. Barish,[12] M. Chadha,[12] S. Chan,[12] D.F. Cowen,[12] G. Eigen,[12] J.S. Miller,[12] C. O'Grady,[12] J. Urheim,[12]
A.J. Weinstein,[12] D. Acosta,[13] M. Athanas,[13] G. Masek,[13] H.P. Paar,[13] J. Gronberg,[14] R. Kutschke,[14] S. Menary,[14]
R.J. Morrison,[14] S. Nakanishi,[14] H.N. Nelson,[14] T.K. Nelson,[14] C. Qiao,[14] J.D. Richman,[14] A. Ryd,[14] H. Tajima,[14]
D. Schmidt,[14] D. Sperka,[14] M.S. Witherell,[14] M. Procario,[15] R. Balest,[16] K. Cho,[16] M. Daoudi,[16] W.T. Ford,[16]
D.R. Johnson,[16] K. Lingel,[16] M. Lohner,[16] P. Rankin,[16] J.G. Smith,[16] J.P. Alexander,[17] C. Bebek,[17]
K. Berkelman,[17] K. Bloom,[17] T.E. Browder,[17,†] D.G. Cassel,[17] H.A. Cho,[17] D.M. Coffman,[17] P.S. Drell,[17]
R. Ehrlich,[17] M. Garcia-Sciveres,[17] B. Geiser,[17] B. Gittelman,[17] S.W. Gray,[17] D.L. Hartill,[17] B.K. Heltsley,[17]
C.D. Jones,[17] S.L. Jones,[17] J. Kandaswamy,[17] N. Katayama,[17] P.C. Kim,[17] D.L. Kreinick,[17] G.S. Ludwig,[17]
J. Masui,[17] J. Mevissen,[17] N.B. Mistry,[17] C.R. Ng,[17] E. Nordberg,[17] J.R. Patterson,[17] D. Peterson,[17] D. Riley,[17]
S. Salman,[17] M. Sapper,[17] F. Würthwein,[17] P. Avery,[18] A. Freyberger,[18] J. Rodriguez,[18] R. Stephens,[18] S. Yang,[18]
J. Yelton,[18] D. Cinabro,[19] S. Henderson,[19] T. Liu,[19] M. Saulnier,[19] R. Wilson,[19] H. Yamamoto,[19] T. Bergfeld,[20]
B.I. Eisenstein,[20] G. Gollin,[20] B. Ong,[20] M. Palmer,[20] M. Selen,[20] J. J. Thaler,[20] A.J. Sadoff,[21] R. Ammar,[22]
S. Ball,[22] P. Baringer,[22] A. Bean,[22] D. Besson,[22] D. Coppage,[22] N. Copty,[22] R. Davis,[22] N. Hancock,[22] M. Kelly,[22]
N. Kwak,[22] H. Lam,[22] Y. Kubota,[23] M. Lattery,[23] J.K. Nelson,[23] S. Patton,[23] D. Perticone,[23] R. Poling,[23]
V. Savinov,[23] S. Schrenk,[23] and R. Wang[23]

(CLEO Collaboration)

[1] *State University of New York at Albany, Albany, New York 12222*
[2] *Ohio State University, Columbus, Ohio 43210*
[3] *University of Oklahoma, Norman, Oklahoma 73019*
[4] *Purdue University, West Lafayette, Indiana 47907*
[5] *University of Rochester, Rochester, New York 14627*
[6] *Southern Methodist University, Dallas, Texas 75275*
[7] *Syracuse University, Syracuse, New York 13244*
[8] *Vanderbilt University, Nashville, Tennessee 37235*
[9] *Virginia Polytechnic Institute and State University, Blacksburg, Virginia 24061*
[10] *Carleton University, Ottawa, Ontario K1S 5B6, Canada
and the Institute of Particle Physics, Canada*
[11] *McGill University, Montréal, Québec H3A 2T8, Canada
and the Institute of Particle Physics, Canada*
[12] *California Institute of Technology, Pasadena, California 91125*
[13] *University of California, San Diego, La Jolla, California 92093*
[14] *University of California, Santa Barbara, California 93106*
[15] *Carnegie-Mellon University, Pittsburgh, Pennsylvania 15213*
[16] *University of Colorado, Boulder, Colorado 80309-0390*
[17] *Cornell University, Ithaca, New York 14853*
[18] *University of Florida, Gainesville, Florida 32611*
[19] *Harvard University, Cambridge, Massachusetts 02138*
[20] *University of Illinois, Champaign-Urbana, Illinois 61801*
[21] *Ithaca College, Ithaca, New York 14850*
[22] *University of Kansas, Lawrence, Kansas 66045*
[23] *University of Minnesota, Minneapolis, Minnesota 55455*
(Received 4 January 1994)

*Permanent address: INP, Novosibirsk, Russia.
†Permanent address: University of Hawaii at Manoa, HI.

We have fully reconstructed decays of both $\bar{B}^0$ and B^- mesons into final states containing either D, D^*, D^{**}, ψ, ψ', or χ_{c1} mesons. This allows us to obtain new results on many physics topics including branching ratios, tests of the factorization hypothesis, color suppression, resonant substructure, and the B^--$\bar{B}^0$ mass difference.

PACS number(s): 13.25.Hw, 13.40.Dk, 14.40.Nd

I. INTRODUCTION

Since B mesons were first fully reconstructed in 1983 by CLEO [1] there have been several papers by CLEO [2,3] and ARGUS [4–6] which reported branching ratios for exclusive decay modes of B mesons. We present here new data from the CLEO II detector using a high resolution photon detector and a much larger data sample than has been available previously.

We are particularly interested in two-body hadronic B meson decays, which occur through the Cabibbo favored $b \rightarrow c$ transition. In these circumstances the dominant weak decay diagram is the spectator diagram, shown in Fig. 1(a). The virtual W^- materializes into either a $\bar{u}d$ or $\bar{c}s$ pair. This pair becomes one of the final state hadrons while the c quark pairs with the spectator antiquark to form the other hadron. The Hamiltonian [7], ignoring hard gluon corrections, is

$$H = \frac{G_F}{\sqrt{2}} V_{cb} \left\{ \left[(\bar{d}u) + (\bar{s}c) \right] (\bar{c}b) \right\} \tag{1}$$

where $(\bar{q}_i q_j) = \bar{q}_i \gamma_\mu (1 - \gamma_5) q_j$, G_F is the Fermi coupling constant, and V_{cb} is the Cabibbo-Kobayashi-Maskawa (CKM) matrix element.

The spectator diagram is modified by hard gluon exchanges between the initial and final quark lines. The effect of these exchanges can be taken into account by use of the renormalization group. These gluons induce an additional term so that the effective Hamiltonian is comprised of two pieces, the original one now multiplied by a coefficient $c_1(\mu)$ and an additional term multiplied by $c_2(\mu)$:

$$H_{\text{eff}} = \frac{G_F}{\sqrt{2}} V_{cb} \left\{ c_1(\mu) \left[(\bar{d}u) + (\bar{s}c) \right] (\bar{c}b) \right.$$
$$\left. + c_2(\mu) \left[(\bar{c}u)(\bar{d}b) + (\bar{c}c)(\bar{s}b) \right] \right\} \tag{2}$$

where the c_i are Wilson coefficients evaluated at the mass scale μ. The Wilson coefficients can be calculated from QCD; however, the calculation of rates is inherently difficult because it is unclear at what scale these coefficients should be evaluated. The usual scale is taken to
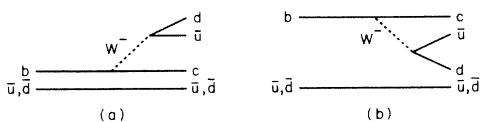
be $\mu \sim m_b^2$. Defining

$$c_\pm(\mu) = c_1(\mu) \pm c_2(\mu), \tag{3}$$

the leading-log approximation gives [8]

$$c_\pm(\mu) = \left(\frac{\alpha_s(M_W^2)}{\alpha_s(\mu)} \right)^{\frac{-6\gamma_\pm}{(33-2n_f)}}, \tag{4}$$

where $\gamma_- = -2\gamma_+ = 2$, and n_f is the number of active flavors, five in this case.

The Hamiltonian in Eq. (2) leads to the "color suppressed" diagram shown in Fig. 1(b), which reflects the quark pairings in the term multiplied by the coefficient $c_2(\mu)$. Observation of $B \rightarrow \psi X_s$ decays, where X_s is a strange meson, gives experimental evidence for the existence of this diagram. Further information on the size of the color suppressed contribution can be obtained from $\bar{B}^0 \rightarrow D^0$ (or D^{*0}) X^0 transitions, where X^0 is a neutral meson containing light quarks. In B^- decays, both types of diagrams are present and can interfere. By comparing the rates for B^- and $\bar{B}^0$ decays, the size and the sign of the color suppressed term can be extracted.

Bjorken has suggested [9] that, in analogy to semileptonic decays, two-body decays of B mesons that occur via the external spectator process can be expressed theoretically as the product of two independent hadronic currents, one describing the formation of a charm meson and the other the hadronization of the $\bar{u}d$ (or $\bar{c}s$) system from the virtual W^-. Qualitatively, he argues that for a B decay with a large energy release the $\bar{u}d$ pair, which is produced as a color singlet, travels fast enough to leave the interaction region without interfering with the formation of the second hadron. The assumption that the amplitude can be expressed as the product of two hadronic currents is called "factorization" in this paper. Several tests of the factorization hypothesis can be made by comparing semileptonic and hadronic B meson decays.

This paper is structured in the following manner. The data sample, detector, and reconstruction procedures are described in Secs. II and III. Branching ratios are given for $B \rightarrow D\pi^-$ and $B \rightarrow D\rho^-$ modes in Sec. IV. In Sec. V results on branching ratios, polarizations, and final state substructure for $B \rightarrow D^*\pi^-$, $B \rightarrow D^*\rho^-$, and $B \rightarrow D^* a_1^-$ are described. Section VI describes a search for D^{**} production in hadronic B decay. This is followed by Sec. VII on exclusive B decays to charmonium, and Sec. VIII on a search for other color suppressed B decays. A $B^- - \bar{B}^0$ mass difference measurement is described in Sec. IX. The interpretation of these results and comparisons to theoretical predictions are discussed in Secs. X (factorization tests), XI (spin symmetry tests), and XII (determination of the color suppressed amplitude).

FIG. 1. B meson decay diagrams: (a) external spectator and (b) color suppressed.

II. DATA SAMPLE AND SELECTION CRITERIA

A. Data sample

The data sample used in this paper was collected with the CLEO II detector at the Cornell Electron Storage Ring (CESR). The integrated luminosity is 0.89 fb^{-1} at the $\Upsilon(4S)$ resonance and 0.41 fb^{-1} at energies just below $B\bar{B}$ threshold, henceforth referred to as the continuum. It is natural to assume equal production of charged and neutral B's since the difference between their masses is very small (see Sec. IX). Then there are a total of equal numbers of $935\,000 \pm 10\,000 \pm 15\,000$ charged and neutral B mesons in this sample.

B. Detector

The CLEO II detector [10] is designed to detect both charged and neutral particles with excellent resolution and efficiency. The detector consists of a charged particle tracking system surrounded by a time-of-flight (TOF) scintillation system and an electromagnetic shower detector with 7800 thallium-doped cesium iodide crystals. In the "barrel," defined as the region where the angle of the shower with respect to the beam axis lies between 32° and 135°, the rms energy resolution is given by $\delta E/E(\%) = 0.35/E^{0.75} + 1.9 - 0.1E$ (E in GeV). In the endcap region, located between 18° and 36° from the beam axis, the rms energy resolution is given by $\delta E/E(\%) = 0.26/E + 2.5$. The tracking system, time-of-flight scintillators, and calorimeter are installed inside a 1.5 T superconducting solenoidal magnet. Immediately outside the magnet are iron and chambers for muon detection. The momentum resolution of the tracking system is given by $(\delta p/p)^2 = (0.0015p)^2 + (0.005)^2$ (p in GeV/c). Ionization loss information (dE/dx), provided by the tracking system, is used to identify charged particles in this analysis. The track must have a dE/dx measurement that differs from that expected for the charged particle hypothesis under consideration by less than 3σ (where henceforth σ denotes the rms resolution).

Muons are identified by a system of drift tubes interleaved with layers of magnet iron. Electron identification utilizes the specific ionization of the track in the drift chamber, the spatial distribution of the energy in the calorimeter, and the ratio of the cluster energy measured in the calorimeter to the track momentum.

C. Photon selection

Photon candidates are selected from showers in the calorimeter barrel that have a minimum energy of 30 MeV, are not matched to a charged particle track from the drift chamber, and have a lateral energy distribution consistent with that expected for photons. In the calorimeter end cap the same criteria are applied but the minimum energy requirement is increased to 50 MeV. A small angular region between 32° and 36° in the barrel-end-cap overlap region is excluded. Neutral pion candi-

TABLE I. D^0 and D^+ decay modes.

D charge	Decay mode	$\mathcal{B}$ (%)	σ_{m_D} (MeV)
D^0	$K^-\pi^+$	$3.91\pm0.08\pm0.17$	8.5
D^0	$K^+\pi^-\pi^0$	12.1 ± 1.1	13.0
D^0	$K^-\pi^+\pi^+\pi^-$	8.0 ± 0.5	8.1
D^+	$K^-\pi^+\pi^+$	9.1 ± 1.4	7.6

dates are selected from pairs of photons with an invariant mass within 2.5σ of the known π^0 mass. These candidates are kinematically fitted with a π^0 mass constraint.

Candidate η mesons are reconstructed in the $\eta \to \gamma\gamma$ mode. They are required to have an invariant mass within 30 MeV of the known η mass (547.5 MeV) [11]. The candidates, which pass the requirements described above, are kinematically constrained to the η mass. Candidate η' mesons are reconstructed in the $\eta\pi^+\pi^-$ channel with $\eta \to \gamma\gamma$. Candidate ω mesons are reconstructed in the $\omega \to \pi^+\pi^-\pi^0$ channel.

D. Charm meson selection

We select D^0, D^+, D^{*+}, and D^{*0} mesons based on the following criteria. Candidate D^0 mesons are identified in the decay modes $D^0 \to K^-\pi^+$, $D^0 \to K^-\pi^+\pi^0$, and $D^0 \to K^-\pi^+\pi^+\pi^-$. Candidate D^+ mesons are selected using the $D^+ \to K^-\pi^+\pi^+$ mode. The decay modes, branching ratios, and rms mass resolutions σ_{m_D} are listed in Table I. We use the CLEO [12] absolute branching ratio for $D^0 \to K^-\pi^+$ decays [13], and the Mark III value for $D^+ \to K^-\pi^+\pi^+$ [14]. We use the Particle Data Group (PDG) values [11] for the ratios $\mathcal{B}(D^0 \to K^-\pi^+\pi^0)/\mathcal{B}(D^0 \to K^-\pi^+)$ (where henceforth $\mathcal{B}$ denotes the branching ratio) and $\mathcal{B}(D^0 \to K^-\pi^+\pi^+\pi^-)/\mathcal{B}(D^0 \to K^-\pi^+)$.

Charged D^* candidates are found using the decay $D^{*+} \to \pi^+D^0$, while neutral D^* candidates are found using the decay $D^{*0} \to \pi^0D^0$. Other D^* decay modes are not used because they have much poorer signal to background ratios. CLEO branching ratios (Table II) are used for D^* decays [15]. We form D^{*+} and D^{*0} candidates by selecting D^0 candidates whose mass is within 2.5σ of the known D^0 mass. Then we require that the D^*-D^0 mass difference be within 2.5σ of the measured values [11,16].

E. Charmonium meson selection

We reconstruct the charmonium states ψ, ψ', and χ_{c1}, where ψ mesons are selected by their decay into pairs of

TABLE II. D^* decay modes used.

D^* mode	$\mathcal{B}$ (%)	$\sigma_{m_{D^*}-m_D}$ (MeV)
$D^{*+} \to D^0\pi^+$	68.1 ± 1.6	0.8
$D^{*0} \to D^0\pi^0$	63.6 ± 4.0	1.1

identified leptons (e^+e^- or $\mu^+\mu^-$). We use the Mark III value [17] $\mathcal{B}(\psi \to l^+l^-) = (5.91 \pm 0.25)\%$ for the ψ to dilepton branching ratio. The kinematics of B decay at the $\Upsilon(4S)$ imply that each lepton in a ψ candidate has a momentum between 0.8 GeV/c and 2.8 GeV/c, with one lepton always having momentum greater than 1.5 GeV/c. For the clean modes $B^- \to \psi K^-$ and $B^0 \to \psi K_S^0$, we obtain good efficiency in the dimuon channel by requiring only one identified muon that penetrates through three interaction lengths. In the dielectron channel, one of the electrons must satisfy a loose electron probability requirement. For modes other than $B^- \to \psi K^-$ and $B^0 \to \psi K_S^0$, both electrons must be identified, or one muon is required to penetrate five interaction lengths and the partner muon is required to penetrate three interaction lengths.

Final state radiation is included in the Monte Carlo simulation of ψ meson decays. For ψ's in the dielectron final states we employ an asymmetric mass cut: $-150 < m(e^+e^-) - m(\psi) < 45$ MeV in order to reduce the efficiency loss from this source. For the dimuon final state, we require $-45 < m(\mu^+\mu^-) - m(\psi) < 45$ MeV since final state radiation is less significant in this case. [The ψ mass resolution would be 15 MeV (rms) in the absence of radiation.] In these mass windows the efficiency for detecting ψ mesons in the dielectron and the dimuon final states are 48.1% and 67.8% for the looser cuts, and are 45.7% and 42.4% when both leptons are identified.

The decay modes $\psi' \to e^+e^-$, $\psi' \to \mu^+\mu^-$, and $\psi' \to \pi^+\pi^-\psi$ are used to select ψ' candidates. The recontruction of the leptonic decays follows the procedure outlined for ψ mesons. Pion candidates for the third decay mode are required to have dE/dx measurements consistent with the pion hypothesis. In addition, tracks that have been identified as part of a K_S^0 decay are rejected. It has been shown that the $\pi^+\pi^-$ invariant mass spectrum from ψ' decays favor larger values relative to that expected from phase space [17]. We require the $\pi^+\pi^-$ invariant mass to be between 0.45 and 0.58 GeV [18]. For ψ' mesons reconstructed through the decay $\psi' \to \pi^+\pi^-\psi$ we require the $\psi' - \psi$ mass difference, $\delta m = m_{\psi'} - m_\psi$, to be between 0.568 and 0.599 GeV. χ_{c1} mesons are reconstructed by their decay into a photon and a ψ meson. We require the photon to be in the good portion of the barrel calorimeter ($|\cos\theta| < 0.71$). If the photon candidate forms an invariant mass within -5 to 3 standard deviations of the known π^0 mass when combined with any other photon in the event, it is rejected.

III. B MESON RECONSTRUCTION PROCEDURES

A. Candidate selection

After selecting D, D^* or charmonium candidates we combine them with one or more additional hadrons to form B candidates. The measured sum of charged and neutral energies E_{meas} of correctly reconstructed B

mesons produced at the $\Upsilon(4S)$ must equal the beam energy E_{beam} to within the experimental resolution. Depending on the B decay mode, $\sigma_{\Delta E}$, the rms resolution on the energy difference $\Delta E = E_{\mathrm{beam}} - E_{\mathrm{meas}}$ varies from 8 to 46 MeV. The modes considered and the corresponding $\sigma_{\Delta E}$ values are given in Tables III–VII and Tables IX–X. We divide the B candidates into a signal sample where ΔE is consistent with zero within 2.5 σ, and a "sideband" sample consisting of two intervals, one with ΔE positive and the other negative, both 2.5σ wide and at least 3σ away from $\Delta E = 0$. For decay modes with large $\sigma_{\Delta E}$, we restrict the sideband width so that the maximum value of ΔE is less than one pion mass. This avoids contamination from the B decay mode with an additional pion. These ΔE sidebands are used to study the background shape.

For B decay modes with a fast ρ^- the energy resolution depends on the momenta of the pions from the ρ^- decay. The momenta of the charged and neutral pions are correlated; a fast π^- accompanies a slow π^0 and vice versa. This correlation is most conveniently formulated as a function of the helicity angle Θ_ρ, the angle in the ρ^- rest frame between the direction of the π^0 and the ρ^- direction in the lab frame. When $\cos\Theta_\rho = +1$, the resolution in the energy measurement is dominated by the calorimeter energy resolution on the fast π^0. In contrast, when $\cos\Theta_\rho = -1$, the largest contribution to the energy resolution comes from the momentum resolution on the fast π^-. Typically $\sigma_{\Delta E}$ varies linearly between 20 MeV at $\cos\Theta_\rho = -1$ and 40 MeV at $\cos\Theta_\rho = 1$. The energy resolution from a Monte Carlo simulation for one such mode ($B^- \to D^0\rho^-$) is shown in Fig. 2 as a function of the ρ^- helicity angle. The energy difference resolutions for modes containing a ρ^- are given in Tables III–VI.

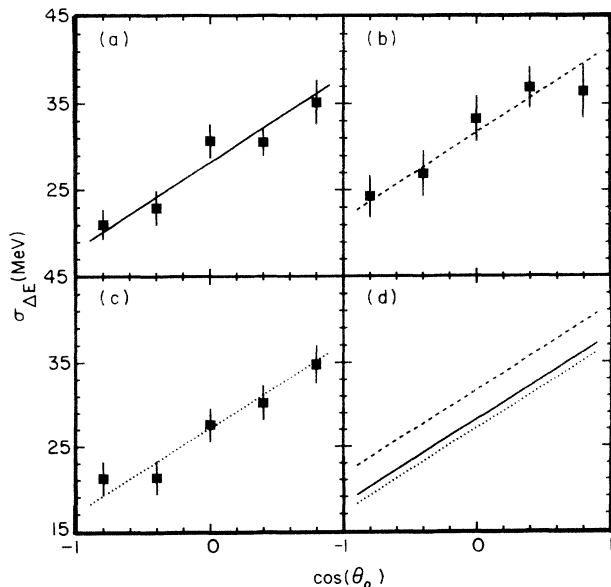In addition to the above selection criteria, events are

FIG. 2. Energy resolution as a function of the ρ^- helicity angle for the decay chains $B^- \to D^0\rho^-$, followed by (a) $D^0 \to K^-\pi^+$, (b) $D^0 \to K^-\pi^+\pi^0$, or (c) $D^0 \to K^-\pi^+\pi^-\pi^+$. The fits for all three modes are shown in (d).

TABLE III. Branching ratios (%) for $B^- \to D^0(n\pi)^-$.

B^- mode	D mode	$\sigma_{\Delta E}$ (MeV)	No. of events	ϵ^a	B (%)	B average (%)
$D^0\pi^-$	$K^-\pi^+$	22	76.3 $\pm$ 9.1	0.433	0.48$\pm$0.06	
	$K^-\pi^+\pi^0$	26	134 $\pm$ 15	0.193	0.62$\pm$0.07	0.55$\pm$0.04$\pm$0.05 $\pm$ 0.02
	$K^-\pi^+\pi^+\pi^-$	20	94$\pm$ 11	0.222	0.57$\pm$0.07	
$D^0\rho^-$	$K^-\pi^+$	18-38	80 $\pm$ 9	0.155	1.40 $\pm$ 0.18	
	$K^-\pi^+\pi^0$	22-42	42 $\pm$ 9	0.036	1.04$\pm$0.23	1.35$\pm$0.12$\pm$0.14 $\pm$ 0.04
	$K^-\pi^+\pi^+\pi^-$	17-37	90.4$\pm$12.1	0.079	1.53$\pm$0.20	

^{a}This efficiency does not include D branching ratios.

TABLE IV. Branching ratios (%) for $\bar{B}^0 \to D^+(n\pi)^-$.

$\bar{B}^0$ mode	D mode	$\sigma_{\Delta E}$ (MeV)	No. of events	ϵ^a	B (%)	B average (%)
$D^+\pi^-$	$K^-\pi^+\pi^+$	20.5	80.6$\pm$9.8	0.32	0.29$\pm$0.04	0.29$\pm$0.04$\pm$0.03 $\pm$ 0.05
$D^+\rho^-$	$K^-\pi^+\pi^+$	18-38	78.9$\pm$10.7	0.12	0.81$\pm$0.11	0.81$\pm$0.11$\pm$0.12 $\pm$ 0.13

^{a}This efficiency does not include D branching ratios.

TABLE V. Branching ratios (%) for $B^- \to D^{*0}(n\pi)$.

B^- mode	D^0 mode	$\sigma_{\Delta E}$ (MeV)	No. of events	ϵ^a	B (%)	B average (%)
$D^{*0}\pi^-$	$K^-\pi^+$	25	13.3$\pm$3.8	0.16	0.36$\pm$0.13	
	$K^-\pi^+\pi^0$	32	37.7$\pm$6.9	0.08	0.63$\pm$0.12	0.52$\pm$0.07$\pm$0.06 $\pm$ 0.04
	$K^-\pi^+\pi^+\pi^-$	21	20.0$\pm$4.9	0.08	0.52$\pm$0.13	
$D^{*0}\rho^-$	$K^-\pi^+$	21-41	25.7$\pm$5.4	0.064	1.74$\pm$0.37	
	$K^-\pi^+\pi^0$	26-46	43.8$\pm$7.8	0.027	2.24$\pm$0.40	1.68$\pm$0.21$\pm$0.25 $\pm$ 0.12
	$K^-\pi^+\pi^+\pi^-$	19-39	16.9$\pm$4.6	0.030	1.19$\pm$0.35	
$D^{*0}\pi^-\pi^-\pi^{+b}$	$K^-\pi^+$	14	5.5$\pm$2.9	0.048	0.51$\pm$0.26	
	$K^-\pi^+\pi^0$	22	27.7$\pm$7.2	0.022	1.74$\pm$0.45	0.94$\pm$0.20$\pm$ 0.16 $\pm$ 0.06
	$K^-\pi^+\pi^+\pi^-$	15	15.0$\pm$4.5	0.025	1.26 $\pm$0.37	

^{a}This efficiency does not include D or D^* branching ratios.
^{b}The three pion mass is required to be between 1.0 GeV and 1.6 GeV consistent with an a_1 meson. (If this channel is dominated by a_1^-, the branching ratio for $D^{*0}a_1^-$ is twice that for $D^{*0}\pi^-\pi^-\pi^+$.)

TABLE VI. Branching ratios (%) for $\bar{B}^0 \to D^{*+}(n\pi)^-$.

$\bar{B}^0$ mode	D^0 mode	$\sigma_{\Delta E}$ (MeV)	No. of events	ϵ^a	B (%)	B average (%)
$D^{*+}\pi^-$	$K^-\pi^+$	25	19.4$\pm$4.5	0.35	0.22$\pm$0.05	
	$K^-\pi^+\pi^0$	32	31.9$\pm$6.4	0.14	0.30$\pm$0.06	0.26$\pm$0.03$\pm$0.04 $\pm$ 0.01
	$K^-\pi^+\pi^+\pi^-$	21	20.5$\pm$5.2.	0.15	0.27$\pm$0.07	
$D^{*+}\rho^-$	$K^-\pi^+$	21.5-41.5	21.9$\pm$5.2	0.12	0.71$\pm$0.17	
	$K^-\pi^+\pi^0$	23-43	39.8$\pm$7.2	0.048	1.08$\pm$0.20	0.74$\pm$0.10$\pm$0.14 $\pm$ 0.03
	$K^-\pi^+\pi^+\pi^-$	20.5-40.5	14.6$\pm$4.6	0.054	0.52$\pm$0.17	
$D^{*+}\pi^-\pi^-\pi^{+b}$	$K^-\pi^+$	14	13.5$\pm$3.9	0.096	0.58$\pm$0.17	
	$K^-\pi^+\pi^0$	22	21.7$\pm$5.9	0.043	0.67$\pm$0.18	0.63$\pm$0.10$\pm$0.11 $\pm$ 0.02
	$K^-\pi^+\pi^+\pi^-$	15	13.9$\pm$4.4	0.042	0.65$\pm$0.19	

^{a}This efficiency does not include D or D^* branching ratios.
^{b}The three pion mass is required to be between 1.0 GeV and 1.6 GeV consistent with an a_1 meson. (If this channel is dominated by a_1^-, the branching ratio for $D^{*+}a_1^-$ is twice that for $D^{*+}\pi^-\pi^-\pi^+$.)

M. S. ALAM *et al.*

required to satisfy $R_2 < 0.5$ where R_2 is the ratio of the second Fox-Wolfram moment to the zeroth moment determined using charged tracks and unmatched neutral showers [19]. A sphericity angle cut is applied to further reduce continuum background. The sphericity angle Θ_s is the angle between the sphericity axis of the particles which form the B candidate and the sphericity axis of the other particles in the event [20]. For a jetlike continuum event, the absolute value of this angle is small; while for a $B\bar{B}$ event, the two axes are almost uncorrelated. Requiring $|\cos\Theta_s| < 0.7$ typically removes about 80% of the continuum background, while retaining 70% of the B decays. The sphericity cut used here depends on the number of pions which accompany the D or D^* meson. For final states with a D^* and a single (2, 3) pion(s) we require $|\cos\Theta_s| < 0.9$ (0.8, 0.7). For all modes which contain a D and a single (2) pion(s) in the final state, we demand that $|\cos\Theta_s| < 0.8$. In modes with ψ mesons, we maximize the efficiency by applying no sphericity angle cut.

To determine the signal yield and display the data we form the beam constrained mass

$$M_B^2 = E_{\text{beam}}^2 - \left(\sum_i \mathbf{p_i}\right)^2, \tag{5}$$

where $\mathbf{p_i}$ is the momentum of the ith daughter of the B candidate. The resolution in this variable is about 2.7 MeV [21] and is about a factor of 10 better than the resolution in invariant mass. The width is dominated by the CESR beam energy spread rather than by detector resolution.

For a specific B decay chain, such as $B^- \to D^0\pi^-, D^0 \to K^-\pi^+\pi^0$, we allow only one candidate per event to appear in the M_B distribution. If there are multiple candidates with $M_B > 5.2$ GeV, the entry with the smallest absolute value of ΔE is selected.

B. Background studies

In order to extract the number of signal events it is crucial to understand the shape of the background in the M_B distributions. There are two contributions to this background, continuum and other $B\bar{B}$ decays. The fraction of background from continuum events varies between about 58% and 91% depending on the B decay mode [22].

We expect that the M_B distribution from the ΔE sidebands will give a good representation of the background shape. To verify this, a Monte Carlo simulation of $B\bar{B}$ events was used to show that the ΔE sidebands can be used to accurately model the shape of the $B\bar{B}$ background under the signal in the beam constrained mass distributions (see Fig. 3). In continuum data, the ΔE sidebands also model the shape of the background in the signal region. The sum of the $B\bar{B}$ Monte Carlo and continuum data agrees in shape with the ΔE sidebands in data (see Fig. 4). Therefore, the ΔE sidebands can be used to model the shape of the background under the signal in data. The M_B distributions for ΔE sidebands in data for several modes are shown in Fig. 5. All
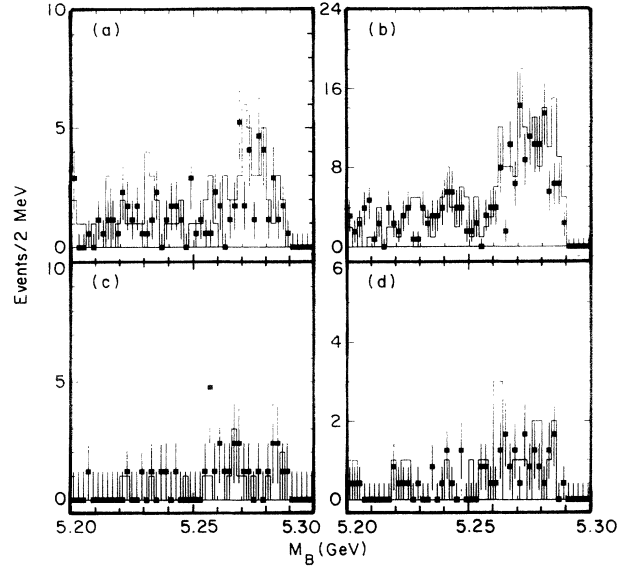

FIG. 3. A Monte Carlo simulation of the M_B distributions of $B\bar{B}$ background (solid histogram), compared with the ΔE sidebands from the same Monte Carlo data (points). All events in the signal modes have been removed from the $B\bar{B}$ Monte Carlo simulation. (a) $B^- \to D^0\pi^-$, (b) $B^- \to D^0\rho^-$. (c) $B^- \to D^{*0}\pi^-$, and (d) $B^- \to D^{*0}\rho^-$.

of these can be fitted with a linear background below $M_B = 5.282$ GeV, and a smooth kinematical cutoff at the end point, which we choose to be parabolic. The distributions of M_B for wrong-sign combinations (e.g., $D^0\pi^+$), wrong-charge combinations (e.g., $D^+\pi^+$), and continuum data can also be adequately fitted with this functional form (henceforth referred to as the CLEO background
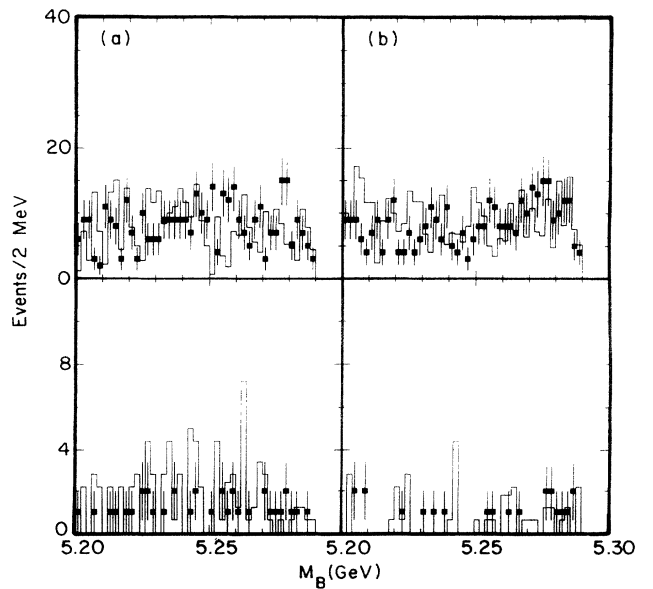

FIG. 4. M_B distributions for ΔE sidebands in on-resonance data (solid histogram) compared to the sum of continuum data and a Monte Carlo simulation of $B\bar{B}$ background (points) (a) $B^- \to D^0\pi^-$, (b) $B^- \to D^0\rho^-$, (c) $B^- \to D^{*0}\pi^-$, and (d) $B^- \to D^{*0}\rho^-$.
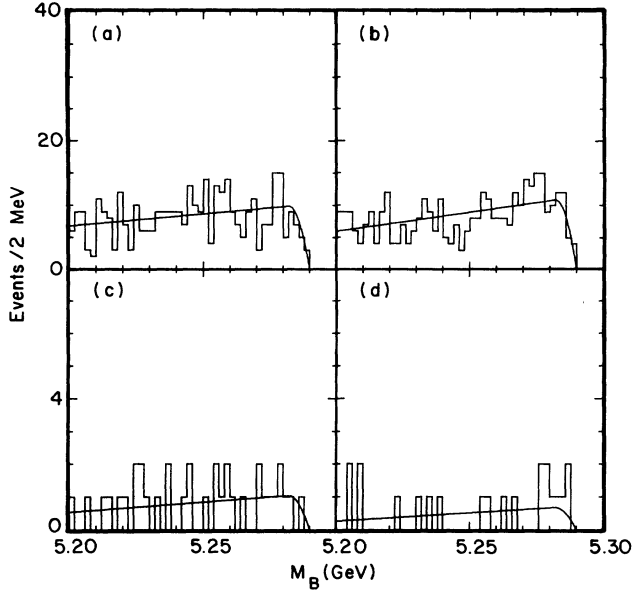
FIG. 5. M_B distributions for ΔE sidebands in data with a fit to the CLEO background shape superimposed: (a) $B^- \to D^0\pi^-$, (b) $B^- \to D^0\rho^-$, (c) $B^- \to D^{*0}\pi^-$, and (d) $B^- \to D^{*0}\rho^-$.

shape). To determine the number of signal events from the M_B spectrum in the ΔE interval centered on zero, we use the background function as determined from the sidebands and a Gaussian signal with a fixed width of 2.64 MeV.

C. Efficiency studies

In order to extract branching ratios, detection efficiencies are determined from a Monte Carlo simulation of the CLEO II detector. The accuracy of the simulation is checked in several ways. We select radiative Bhabha events ($e^+e^- \to e^+e^+\gamma$) using only calorimeter information and then embed the tracks into hadronic events. We find that the efficiency for the detection of charged tracks above 225 MeV/c is correct to better than 2%. The Monte Carlo simulation of charged tracks with transverse momenta below 225 MeV/c is more complicated since these tracks do not traverse the entire drift chamber. The accuracy of the simulation is verified using the D^* decay angle distribution of inclusive $D^{*+} \to D^0\pi^+$, $D^0 \to K^-\pi^+$ decays which must be symmetric after efficiency correction. The simulation of low p_T tracks agrees with the Monte Carlo simulation for $100 < p < 225$ MeV/c. However, the efficiency for tracks in this momentum range is known to only $\pm5\%$.

The accuracy of the photon detection efficiency can be verified by comparing the ratio of branching ratios of $\eta \to \pi^0\pi^0\pi^0$ and $\eta \to \gamma\gamma$ to the average ratio given by the PDG [11]. This test indicates that the single photon efficiency is modeled to better than $\pm2.5\%$. Other checks of the π^+ and π^0 detection efficiency are performed by comparing the yield of fully reconstructed $D^0 \to K^-\pi^+\pi^0$ decays with the yield of partially reconstructed $D^0 \to$

$K^-\pi^0(\pi^+)$ where the π^+ is not detected. Additional consistency checks have been performed by comparing inclusive D^{*+} and D^{*0} cross sections in the continuum, and by comparing the ratios $\mathcal{B}(D^0 \to K^-\pi^+\pi^-\pi^+)$ $/\mathcal{B}(D^0 \to K^-\pi^+)$ and $\mathcal{B}(\eta \to \pi^-\pi^+\pi^0)/\mathcal{B}(\eta \to \gamma\gamma)$ to the values in the PDG compilation [11].

IV. BRANCHING RATIOS FOR $D\pi^-$ AND $D\rho^-$ FINAL STATES

We reconstruct the decay modes $\bar{B}^0 \to D^+\pi^-$, $\bar{B}^0 \to D^+\rho^-$, $B^- \to D^0\pi^-$, and $B^- \to D^0\rho^-$ following the procedures described in Secs. II and III. There is an additional complication for the analysis of the $B \to D\rho^-$ modes. Events consistent with the decay chain $B \to D^*\pi^-$, $D^* \to D\pi^0$ have the same final state particles and thus form a potential background. We eliminate this background by discarding events for which the $D^* - D$ mass difference is consistent with the D^* hypothesis. This veto does not reduce the efficiency for $B \to D\rho^-$. A Monte Carlo simulation of $B\bar{B}$ decays shows a broad enhancement in the signal region for $B^- \to D^0\pi^-$ and $B^- \to D^0\rho^-$ (see Fig. 3). This enhancement contains contributions from $B \to D^{*0}X$, $D^{*0} \to D^0\gamma$ transitions which can be modeled with the CLEO background shape.

To select $B \to D\rho^-$ channels we impose additional requirements on the $\pi^-\pi^0$ invariant mass and decay angle. Specifically, we require that $|m(\pi^-\pi^0) - 770| < 150$ MeV/c^2. Since the decay $B \to D\rho^-$ is fully longitudinally polarized (helicity zero due to angular momentum conservation), a cut on the ρ helicity angle is imposed ($|\cos\Theta_\rho| > 0.4$) [23]. The beam constrained mass distributions for $B \to D\pi^-$ and $B \to D\rho^-$ are shown in Fig. 6. Figure 7 shows the ρ helicity angle distributions (with the cut on the helicity angle removed) for $\bar{B}^0 \to D^+\rho^-$ and
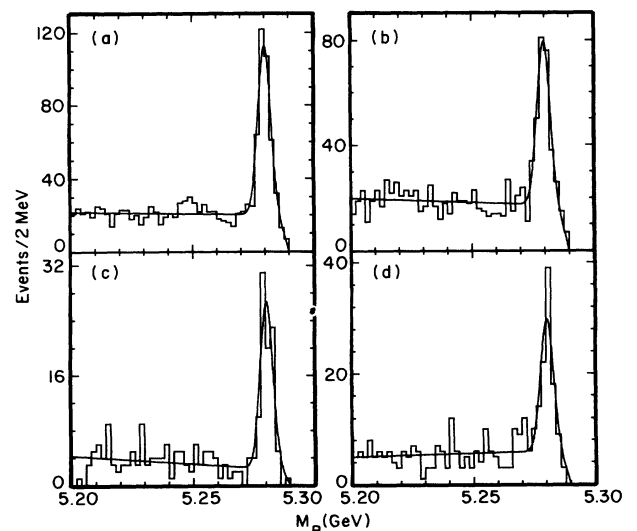

FIG. 6. The beam constrained mass distributions for (a) $B^- \to D^0\pi^-$, (b) $B^- \to D^0\rho^-$ for $|\cos\Theta_\rho| > 0.4$, (c) $\bar{B}^0 \to D^+\pi^-$, and (d) $\bar{B}^0 \to D^+\rho^-$ for $|\cos\Theta_\rho| > 0.4$.

for $B^- \to D^0 \rho^-$ after B mass sideband subtraction. After efficiency correction, these distributions are given by the functional form

$$\frac{dN}{d\cos\Theta_\rho} = \frac{\Gamma_L}{\Gamma}\cos^2\Theta_\rho + 0.5\left(1 - \frac{\Gamma_L}{\Gamma}\right)\sin^2\Theta_\rho, \quad (6)$$

where Γ_L/Γ is the fraction of longitudinal polarization. The fit gives $\Gamma_L/\Gamma = 1.07 \pm 0.05$ for $B^- \to D^0\rho^-$ and $\Gamma_L/\Gamma = 0.92 \pm 0.07$ for $\bar{B}^0 \to D^+\rho^-$. These results are consistent with full polarization as expected and thus provide a consistency check of the background subtraction and efficiency correction. Monte Carlo simulation shows that most of the $B\bar{B}$ backgrounds in $B \to D\rho^-$ decays are due to combinations with an incorrectly reconstructed low momentum π^0. Therefore a fit to the beam constrained mass distribution with $\cos\Theta_\rho < -0.4$ is also performed as a consistency check of the analysis [24]. These results agree with the branching ratios obtained using the full range of helicity angle.

The $\pi^-\pi^0$ invariant mass distribution for the B signal region (± 6.5 MeV of the nominal B mass) is shown in Figs. 8 and 9 after B sideband subtraction. Fitting this distribution to the sum of a Breit-Wigner term and a parametrization of nonresonant $B \to D\pi^-\pi^0$ decay [25] we find that fewer than 2.5% (at 90% C.L.) of the events in the B mass peak arise from nonresonant decays, after applying the helicity angle cut and restricting the $\pi^-\pi^0$ mass to lie in the ρ mass region. The observed $D\pi^-\pi^0$ events are consistent with $B \to D\rho^-$ and any nonresonant contribution can be neglected.

The resulting branching ratios for $B \to D\pi^-$ and $B \to D\rho^-$ are given in Tables III and IV.

Two systematic errors are quoted on the branching ratios. The first includes contributions from background shape ($\sim 5\%$), Monte Carlo statistics ($2 - 4\%$), and the
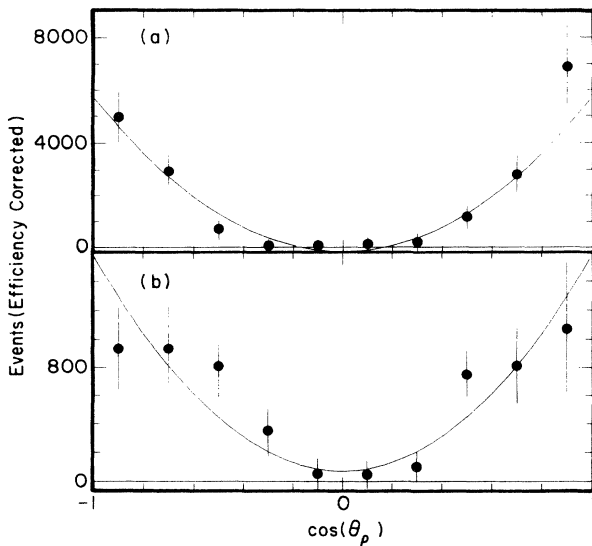

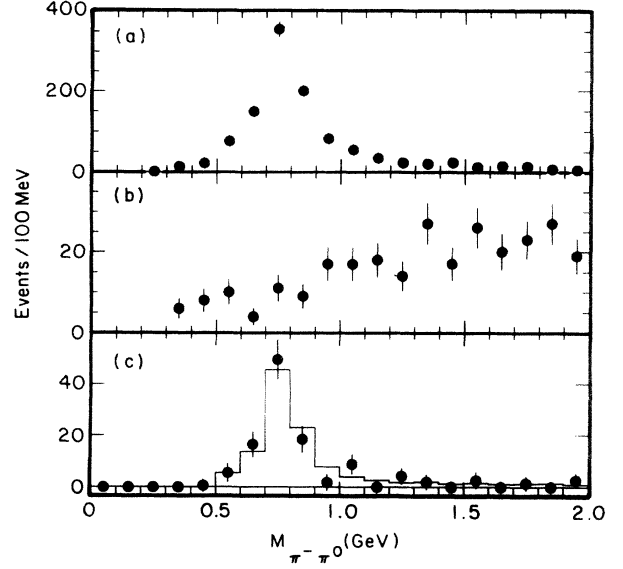FIG. 8. (a) The $\pi^0\pi^-$ invariant mass spectrum for a $\bar{B}^0 \to D^+\rho^-$ Monte Carlo simulation. (b) The $\pi^0\pi^-$ invariant mass spectrum $\bar{B}^0 \to D^+(\pi^-\pi^0)_{NR}$ Monte Carlo simulation. (c) The $\pi^0\pi^-$ invariant mass spectrum for the $\bar{B}^0 \to D^+\pi^0\pi^-$ mode in data.

uncertainty in the modeling of the tracking and π^0 detection efficiencies (which depend on the multiplicity of the decay mode as described earlier) and the relative D^0 branching fractions. The second systematic error contains the errors from the $D^+ \to K^-\pi^+\pi^+$ ($\pm 14\%$) and $D^0 \to K^-\pi^+$ absolute branching ratios ($\pm 2.7\%$).

FIG. 7. The efficiency corrected ρ helicity angle distributions: (a) $B^- \to D^0\rho^-$ and (b) $\bar{B}^0 \to D^+\rho^-$ after B mass sideband subtraction.

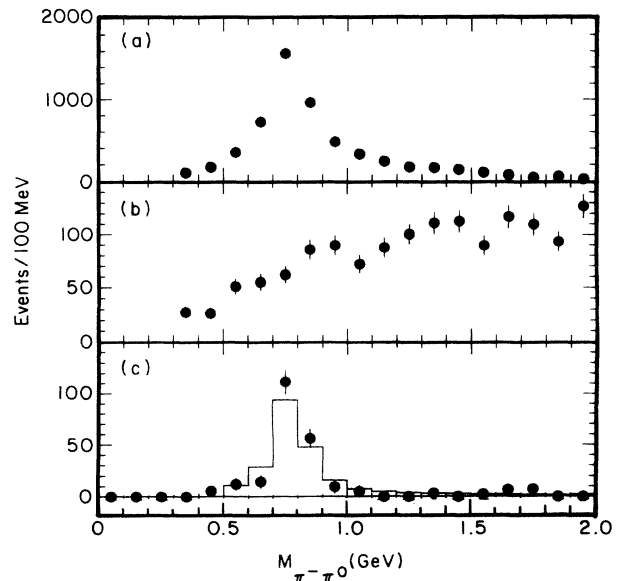FIG. 9. (a) The $\pi^0\pi^-$ invariant mass spectrum for a $B^- \to D^0\rho^-$ Monte Carlo simulation. (b) The $\pi^0\pi^-$ invariant mass spectrum $B^- \to D^0(\pi^-\pi^0)_{NR}$ Monte Carlo simulation. (c) The $\pi^0\pi^-$ invariant mass spectrum for the $B^- \to D^0\pi^0\pi^-$ mode in data.

V. MEASUREMENTS OF $D^*(N\pi)^-$ FINAL STATES

A. Branching ratios

We now consider final states containing a D^* meson and one, two, or three pions. These include the $B \to D^*\pi^-$, $B \to D^*\rho^-$, and $B \to D^*a_1^-$ decay channels. A cut on the D^* helicity angle, $|\cos\theta_{D^*}| > 0.4$, is made for $B \to D^*\pi$ but not for $D^*\rho$ and D^*a_1. The beam constrained mass distributions for the $\bar{B}^0 \to D^{*+}\pi^-$ and $B^- \to D^{*0}\pi^-$ are shown in Fig. 10. Our results for the decays $\bar{B}^0 \to D^{*+}\pi^-$ and $B^- \to D^{*0}\pi^-$ are listed in Tables V and VI. The first error quoted on the branching ratios is statistical, followed by two systematic errors. The first systematic error contains contributions from the uncertainties in the efficiency for charged track finding, the uncertainty in photon detection, variations in event yield from changes in background shape, Monte Carlo statistics, and the relative D^0 branching fractions. The second systematic error contains the errors on the $D^0 \to K^-\pi^+$ and $D^* \to D^0\pi$ branching ratios.

Figure 10 shows the beam constrained mass distributions for the $\bar{B}^0 \to D^{*+}\rho^-$ and $B^- \to D^{*0}\rho^-$. To study the resonant substructure in $\bar{B}^0 \to D^{*+}\pi^-\pi^0$ the cut on the $\pi^-\pi^0$ mass is removed. For events in the B signal region ($|M_B - 5.280| < 0.006$ GeV) the $\pi^-\pi^0$ spectrum is examined after subtracting the $\pi^-\pi^0$ spectrum from the low B mass sideband ($5.2 < M_B < 5.26$ GeV). The background-subtracted $\pi^-\pi^0$ invariant mass spectrum is then fitted to the sum of a Breit-Wigner term and a polynomial parametrization of the nonresonant $\bar{B}^0 \to D^{*+}\pi^-\pi^0$ obtained from a Monte Carlo simulation. Figure 11 shows the fit to the background-subtracted $\pi^-\pi^0$ invariant mass spectrum. The fit gives an upper limit of less than six nonresonant $\bar{B}^0 \to D^{*+}\pi^-\pi^0$ events in the ρ mass window at the 90% confidence level. This implies
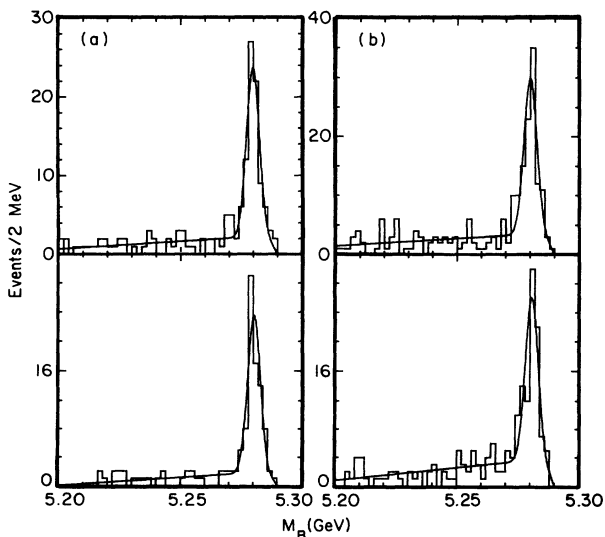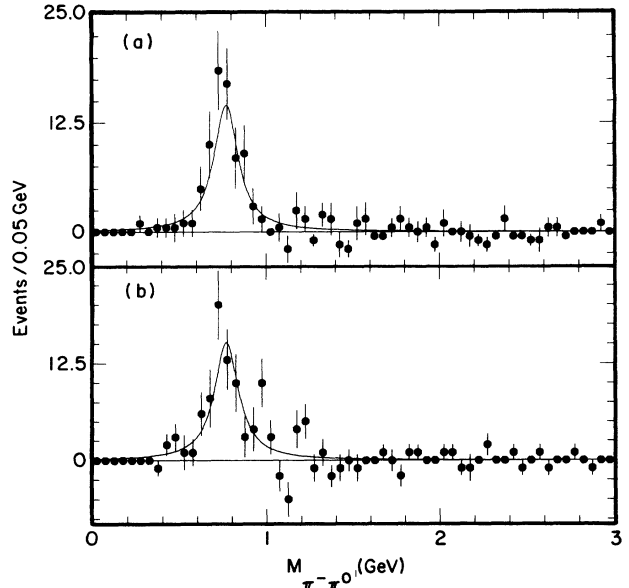
FIG. 11. (a) The $\pi^0\pi^-$ invariant mass spectrum for the $\bar{B}^0 \to D^{*+}\pi^0\pi^-$ decay mode. (b) The $\pi^0\pi^-$ invariant mass spectrum for the $\bar{B}^- \to D^{*0}\pi^0\pi^-$ decay mode.

that the nonresonant contribution to the $\bar{B}^0 \to D^{*+}\rho^-$ decay is less than 9% at the 90% confidence level. If we instead take the shape of the nonresonant component from a $D^{**}(2420)\pi^+$ Monte Carlo simulation we obtain a similar limit for the non-ρ component. A similar study has been made of $B^- \to D^{*0}\rho^-$ which also shows a negligible nonresonant component. The branching ratios for $B \to D^*\rho$ can be found in Tables V and VI. In Fig. 12 we show the M_B distributions for $B^- \to D^{*0}\pi^-\pi^-\pi^+$ and $\bar{B}^0 \to D^{*+}\pi^-\pi^-\pi^+$ where the $\pi^-\pi^-\pi^+$ invariant mass is required to be in the interval $1.0 < \pi^-\pi^-\pi^+ < 1.6$ GeV. To show that this signal arises dominantly from a_1^- we also present the M_B distributions for the a_1 sidebands $0.6 < \pi^-\pi^-\pi^+ < 0.9$ GeV and $1.7 < \pi^-\pi^-\pi^+ < 2.0$ GeV (Fig. 13), where there are signals of 15 ± 6 and 0 ± 5.5 events for the D^{*+} and D^{*0} channels respectively. The sideband signals are $18\pm6\%$ (0 ± 13 %) of the signals in the a_1 peak, as compared to the expectation of about 10% from the tails of a Breit-Wigner distribution. In Figs. 14 and 15 we show the $\pi^-\pi^-\pi^+$ mass distributions for a $B \to D^*a_1^-$ Monte Carlo simulation, a $B \to D^*\pi^-\rho^0$ nonresonant background simulation, and the data events

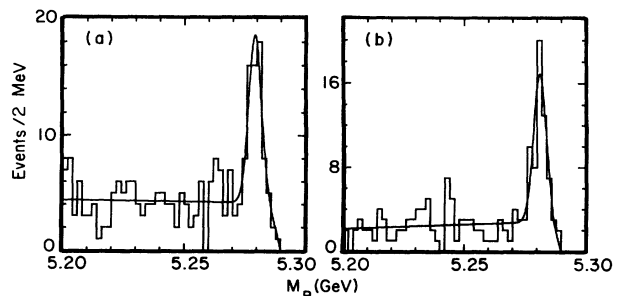FIG. 10. Beam-constrained mass distributions for (a) $B^- \to D^{*0}\pi^-$, (b) $B^- \to D^{*0}\rho^-$, (c) $\bar{B}^0 \to D^{*+}\pi^-$, and (d) $\bar{B}^0 \to D^{*+}\rho^-$.

FIG. 12. Beam constrained mass distributions for (a) $B^- \to D^{*0}a_1^-$ and (b) $\bar{B}^0 \to D^{*+}a_1^-$.
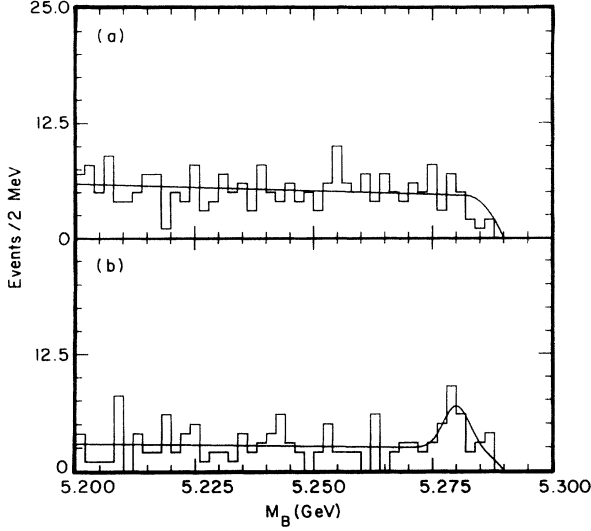
FIG. 13. The M_B distributions for (a) $B^- \to D^{*0}\pi^-\pi^-\pi^+$ and $\bar{B}^0 \to D^{*+}\pi^-\pi^-\pi^+$, where the $\pi^-\pi^-\pi^+$ invariant mass is required to be in the a_1^- mass sidebands.

in the B signal region with the scaled B mass sideband subtracted. The a_1 meson is parametrized in the Monte Carlo simulation as a Breit-Wigner resonance shape with $m_{a_1} = 1182$ MeV and $\Gamma_{a_1} = 466$ MeV. The fit gives upper limits of less than 4.2 and 4.6 nonresonant events at the 90% confidence level. This implies that the non-resonant components in this decay are less than 9.4% and 10.6% at the 90% confidence level. We have verified that a $D^{**}(2420)\rho^-$ Monte Carlo simulation gives a similar
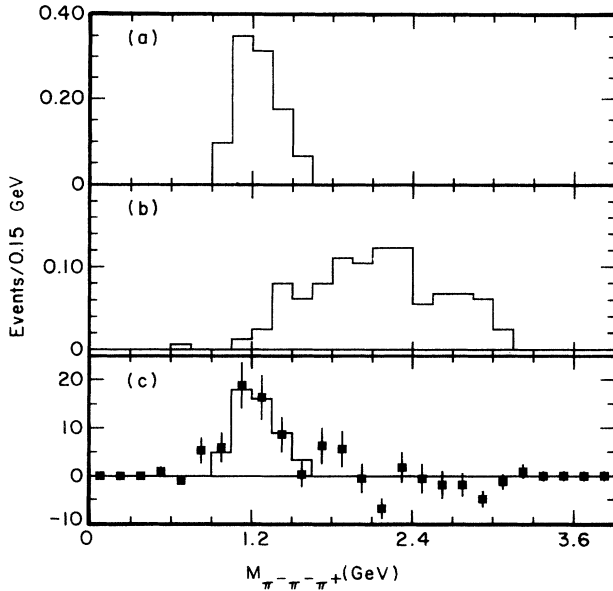

FIG. 14. (a) The $\pi^-\pi^-\pi^+$ invariant mass spectrum from a Monte Carlo simulation of $\bar{B}^0 \to D^{*+}a_1^-$. (b) The $\pi^-\pi^-\pi^+$ invariant mass spectrum from Monte Carlo simulation for $\bar{B}^0 \to D^{*+}(\pi^-\rho^0)_{\mathrm{NR}}$. (c) The $\pi^-\pi^-\pi^+$ mass spectrum from data after B mass sideband subtraction (points). The fit to the sum of (a) and (b) is superimposed (histogram).

FIG. 15. (a) The $\pi^-\pi^-\pi^+$ invariant mass spectrum from a Monte Carlo simulation of $\bar{B}^- \to D^{*0}a_1^-$. (b) The $\pi^-\pi^-\pi^+$ invariant mass spectrum from Monte Carlo simulation for $\bar{B}^- \to D^{*0}(\pi^-\rho^0)_{\mathrm{NR}}$. (c) The $\pi^-\pi^-\pi^+$ mass spectrum from data after B mass sideband subtraction (points). The fit to the sum of (a) and (b) is superimposed (histogram).
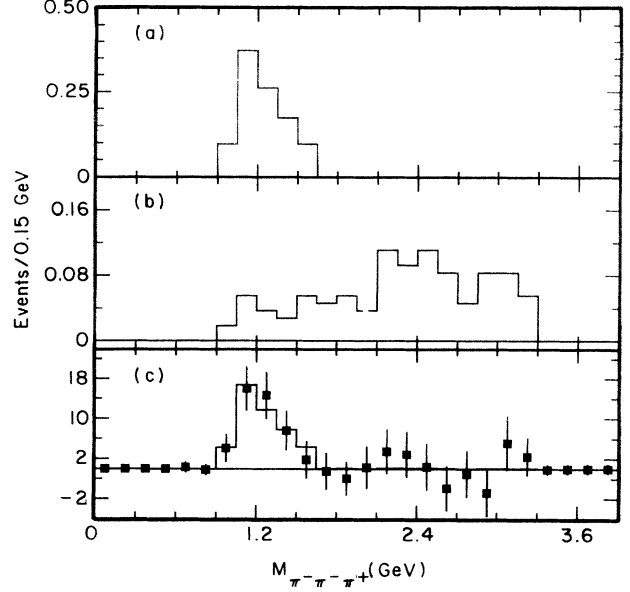
limit for the non-a_1 component. Our results for B meson decays into final states containing a D^* meson and three charged pions are also listed in Tables V and VI.

B. Polarization in $B \to D^{*+}\rho^-$ decays

The sample of fully reconstructed $B \to D^{*+}\rho^-$ decays can be used to measure the D^{*+} and ρ^- polarizations. By comparing the measured polarizations in $\bar{B}^0 \to D^{*+}\rho^-$ with the expectation from the corresponding semileptonic B decay a test of the factorization hypothesis can be performed (see Sec. X C).

The polarization is obtained from the helicity angle distribution. The ρ helicity angle Θ_ρ was defined earlier. The D^{*+} helicity angle Θ_{D^*} is the angle between the π^+ direction and B direction in the D^{*+} rest frame.

The momentum in the laboratory for pions from the D^{*+} decay which are emitted in the backward hemisphere ($\cos\Theta_{D^*} < 0$ in our convention) extends from 160 MeV/c down to about 100 MeV/c. In this momentum range, the reconstruction efficiency for charged tracks is reduced and becomes momentum dependent.

Before examining the $\bar{B}^0 \to D^{*+}\rho^-$ decay mode, we perform a consistency check of the efficiency correction and analysis procedure by measuring the polarization in $\bar{B}^0 \to D^{*+}\pi^-$. Since B mesons and pions are pseudoscalars, the D^{*+} mesons from the decay $\bar{B}^0 \to D^{*+}\pi^-$ will be longitudinally polarized giving a $\cos^2\Theta_{D^*}$ distribution. The same procedure used in the analysis of the

$\bar{B}^0 \to D^{*+}\rho^-$ polarization is applied to this case. After performing the sideband subtraction and correcting for efficiency [26], we obtain the D^{*+} helicity angle distribution shown in Fig. 16(c). A fit to this distribution gives $\Gamma_L/\Gamma = 106\pm7\%$ which is consistent with the expectation

from angular momentum conservation of $\Gamma_L/\Gamma = 100\%$.

We now proceed to measure the polarization in $\bar{B}^0 \to D^{*+}\rho^-$ decays. After integration over χ, the angle between the normals to the D^{*+} and the ρ^- decay planes, the helicity angle distribution can be expressed as [27]

$$\frac{d^2\Gamma}{d\cos\Theta_{D^*} d\cos\Theta_\rho} \propto \frac{1}{4}\sin^2\Theta_{D^*}\sin^2\Theta_\rho(|H_{+1}|^2 + |H_{-1}|^2) + \cos^2\Theta_{D^*}\cos^2\Theta_\rho|H_0|^2. \tag{7}$$

The fraction of longitudinal polarization is defined by [27]

$$\frac{\Gamma_L}{\Gamma} = \frac{|H_0|^2}{|H_{+1}|^2 + |H_{-1}|^2 + |H_0|^2}. \tag{8}$$

If longitudinal polarization dominates, both the D^{*+} and the ρ^- helicity angles will follow a $\cos^2\Theta$ distribution, whereas in the case of transverse polarization we will observe a $\sin^2\Theta$ distribution for both helicity angles.

To measure the polarization we combine the helicity angle distributions for the three D^0 submodes in the B signal region (defined by $|M_B - 5.280| < 0.006$ GeV) and then subtract the helicity angle distribution of the scaled sideband (defined by $5.200 < M_B < 5.260$ GeV). We fit the resulting helicity angle distributions to the functional form given in Eq. (6).

From the fit to the D^{*+} helicity angle distribution, we find $\Gamma_L/\Gamma = (85 \pm 8)\%$, and from the corresponding fit to the ρ helicity angle distribution we find $\Gamma_L/\Gamma =$
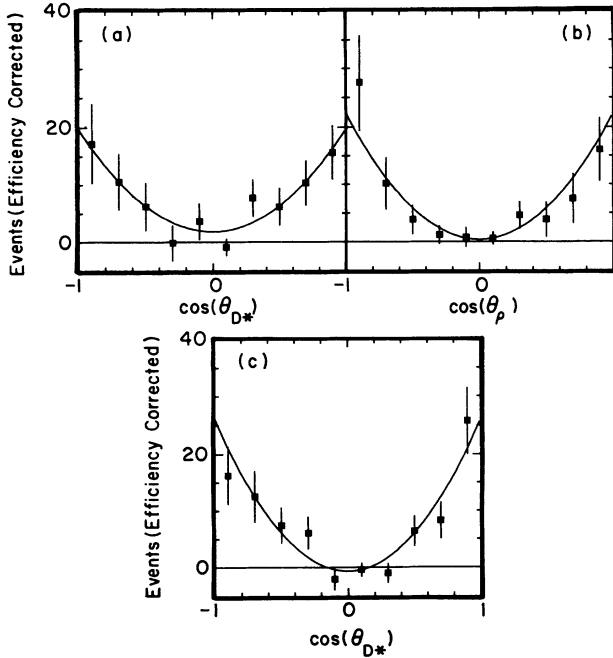
$(97 \pm 8)\%$. The results of the fits [28] are shown in Fig. 16(a) and 16(b). The statistical error can be reduced by taking advantage of the correlation between the two helicity angles (see Fig. 17). The most precise result can be extracted by performing an unbinned two-dimensional likelihood fit to the joint $(\cos\Theta_{D^*}, \cos\Theta_\rho)$ distribution. This method gives

$$(\Gamma_L/\Gamma)_{\bar{B}^0 \to D^{*+}\rho^-} = (93 \pm 5 \pm 5)\%. \tag{9}$$

The systematic error contains the uncertainties due to the background parametrization and the detector acceptance.

VI. MEASUREMENTS OF D^{**} FINAL STATES

In addition to the production of D and D^* mesons, the charm quark and spectator antiquark can also hadronize as a D^{**} meson. The $D^{**0}(2460)$ has been observed experimentally and identified as the $J^P = 2^+$ state, while the $D^{**0}(2420)$ has been identified as the 1^+ state [11]. These states have full widths of approximately 20 MeV. Two other states, a 0^+ and another 1^+ are predicted but have not yet been observed. Presumably this is due to their large intrinsic widths. There is evidence for D^{**} production in semileptonic B decays [29,30], and it is

FIG. 16. (a) Helicity angle from $D^{*+} \to D^0\pi^+$ in $\bar{B}^0 \to D^{*+}\rho^-$ and (b) helicity angle from $\rho^- \to \pi^-\pi^0$ in $\bar{B}^0 \to D^{*+}\rho^-$. (c) Helicity angle from $D^{*+} \to D^0\pi^+$ in $\bar{B}^0 \to D^{*+}\pi^-$. The data have been corrected for efficiency and background subtracted. The curves are the results of the fit described in the text.
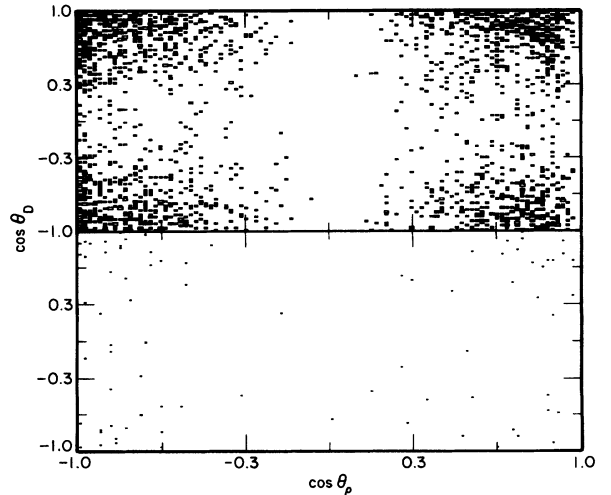

FIG. 17. (a) Monte Carlo simulation of D^{*+} helicity angle versus ρ^- helicity angle for longitudinally polarized $\bar{B}^0 \to D^{*+}\rho^-$. (b) Data for D^{*+} helicity angle versus ρ^- helicity angle for candidates in $\bar{B}^0 \to D^{*+}\rho^-$.

possible that the D^{**} can also be seen in hadronic B decays.

In order to search for D^{**} mesons from B decays we first study the final states $B^- \to D^{*+}\pi^-\pi^-$ and $B^- \to D^{*+}\pi^-\pi^-\pi^0$. In the latter case we require that one $\pi^-\pi^0$ invariant mass is consistent with the ρ^- mass. The reactions $B^- \to D^{*+}\pi^-\pi^-$ and $B^- \to D^{*+}\pi^-\pi^-\pi^0$ have not been observed clearly in past experiments [3,6] and are not expected to occur in a simple picture in which the c quark plus spectator antiquark form a D^*. We combine the D^{*+} with a π^- to form a D^{**} candidate. D^{**} candidates lying within one full width of the nominal mass of either a $D^{**0}(2420)$ or a $D^{**0}(2460)$ are then combined with a π^- or ρ^- to form a B^- candidate.

We have also searched for D^{**} production in the channels $D^+\pi^-\pi^-$ and $D^0\pi^-\pi^+$. Since $D^{**0}(2420) \to D\pi$ is forbidden, we only search for $D^{**0}(2460)$ in the $D\pi\pi$ final state. For this subset of modes, we require the $D\pi$ mass to lie within $\pm 1.5\,\Gamma$ (±28 MeV) of the nominal $D^{**}(2460)$ mass.

Figures 18 and 19 show the B mass distributions for combinations of $D^{**0}(2460)$ or $D^{**0}(2420)$, and π^- or ρ^-. In the $D^{**0}(2420)\pi^-$ mode, there is an excess of 8.5 events in the B peak region with an estimated background of 1.5 events. The binomial probability that the excess is due to a background fluctuation is 4×10^{-6}, which indicates that this is a significant signal. In this channel we give the branching ratio in Table VII, while for the other five combinations where the probability that the observed events are the result of a background fluctuation is larger, we give upper limits. Our results are consistent with theoretical predictions [31,32] based on the factorization hypothesis (Table VIII).

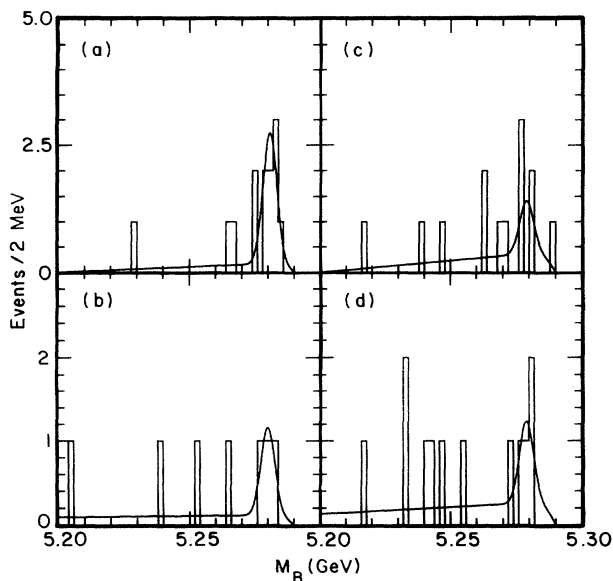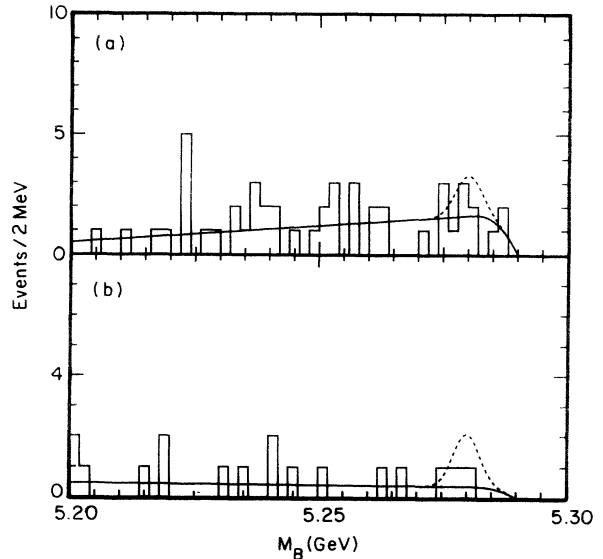We have also investigated the final states $D^{*+}\pi^-\pi^-$

FIG. 19. Beam-constrained mass distributions for (a) $B^- \to D^{**0}(2460)\pi^-$ where $D^{**0}(2460) \to D^+\pi^-$, and (b) $\bar{B}^0 \to D^{**+}(2460)\pi^-$ where $D^{**+}(2460) \to D^0\pi^+$. The curve is the result of the fit and the dotted line is the 90% confidence level upper limit.

($D^+\pi^-\pi^-$ and $D^0\pi^+\pi^-$) where the $D^{(*)}$ and a charged pion are not constrained to lie in any particular mass interval. To observe these signals, the background from the final states $D^{(*)}\rho^-$ must be suppressed. Since the $D^{(*)}\rho^-$ final state is highly polarized (see Sec. V B), it is possible that the slow π^0 from the ρ^- decay can be exchanged for a slow charged pion from the decay of the other B meson. To eliminate this background, we make cuts on the cosines of the helicity angles Θ_{D^*} and $\Theta_{D^{**}}$, where $\Theta_{D^{**}}$ is calculated for the $D^{*+}\pi^-_{\rm slow}$ system with $\pi^-_{\rm slow}$ being the slower π^- of the two. This helicity angle is defined as the angle between the B and the fast π^- in the rest frame of $D^{*+}\pi^-_{\rm slow}$ system. We require $\cos\Theta_{D^{**}} < 0.8$ and $|\cos\Theta_{D^*}| < 0.7$. For the $B \to D\pi\pi$ modes, a similar cut, $\cos\Theta_\rho < 0.7$, is made using the $\pi\pi$ system. In Figs. 20 and 21, we show the M_B candidate mass distributions. There is a significant signal in $B \to D^{*+}\pi^-\pi^-$. For the other two modes we quote upper limits in Table VII.

VII. EXCLUSIVE $B \to$ CHARMONIUM DECAYS

A. Introduction

In B decays to charmonium the c quark from the b combines with a $\bar{c}$ quark from the virtual W^- to form a charmonium state. This process is described by the color-suppressed diagram shown in Fig. 1(b). By comparing B meson decays to different final states with charmonium mesons the dynamics of this decay mechanism can be investigated. The decay modes $\bar{B}^0 \to \psi K^0$ and $\bar{B}^0 \to \psi' K^0$ are of special interest since the final states are CP eigenstates which can be used to determine one of the three CP-violating angles accessible to study in B

FIG. 18. Beam constrained mass distributions for (a) $B^- \to D^{**0}(2420)\pi^-$ where $D^{**0}(2420) \to D^{*+}\pi^-$, (b) $B^- \to D^{**0}(2460)\pi^-$ where $D^{**0}(2460) \to D^{*+}\pi^-$, (c) $B^- \to D^{**0}(2420)\pi^-\pi^0$ where $D^{**0}(2420) \to D^{*+}\pi^-$, (d) $B^- \to D^{**0}(2460)\pi^-\pi^0$ where $D^{**0}(2460) \to D^{*+}\pi^-$.

TABLE VII. Branching ratios (%) for $B \to D^{**}(n\pi)$.

B mode	*D* mode	$\sigma_{\Delta E}$ (MeV)	ϵ^{a}	No. of events	*B* average (%)
$D^0\pi^+\pi^-$	$K^-\pi^+$	17	0.19	< 10.1	< 0.16
$D^+\pi^-\pi^-$	$K^-\pi^+\pi^+$	15.5	0.11	< 10.3	< 0.14
$D^{**}(2460)\pi^- \to D^+\pi^-\pi^-$	$K^-\pi^+\pi^+$	16	0.21	< 5.6	< 0.13
$D^{**}(2460)\pi^- \to D^0\pi^+\pi^-$	$K^-\pi^+$	17	0.26	< 5.6	< 0.22
$D^{**}(2460)\rho^- \to D^+\pi^-\pi^-\pi^0$	$K^-\pi^+\pi^+$	16	0.08	< 6.1	< 0.47
$D^{**}(2460)\rho^- \to D^0\pi^+\pi^-\pi^0$	$K^-\pi^+$	17	0.11	< 5.1	< 0.49
$D^*\pi^-\pi^-$	$K^-\pi^+$	16	0.161		
	$K^-\pi^+\pi^0$	23	0.061	14.1 ± 5.4	$0.19 \pm 0.07 \pm 0.03 \pm 0.01$
	$K^-\pi^+\pi^-\pi^+$	19	0.075		
$D^{**}(2420)\pi^- \to D^{*+}\pi^-\pi^-$	$K^-\pi^+$	16	0.161		
	$K^-\pi^+\pi^0$	23	0.061	8.5 ± 3.8	$0.11 \pm 0.05 \pm 0.02 \pm 0.01$
	$K^-\pi^+\pi^-\pi^+$	19	0.075		
$D^{**}(2460)\pi^- \to D^{*+}\pi^-\pi^-$	$K^-\pi^+$	16	0.161		
	$K^-\pi^+\pi^0$	23	0.061	3.5 ± 2.3	< 0.28
	$K^-\pi^+\pi^-\pi^+$	19	0.075		
$D^{**}(2420)\rho^- \to D^{*+}\pi^-\pi^-\pi^0$	$K^-\pi^+$	30	0.078		
	$K^-\pi^+\pi^0$	24	0.037	3.4 ± 2.1	< 0.14
	$K^-\pi^+\pi^-\pi^+$	27	0.042		
$D^{**}(2460)\rho^- \to D^{*+}\pi^-\pi^-\pi^0$	$K^-\pi^+$	30	0.078		
	$K^-\pi^+\pi^0$	24	0.037	3.2 ± 2.4	< 0.5
	$K^-\pi^+\pi^+\pi^-$	27	0.042		

ªThe efficiencies do not include the branching ratios for D, D^*, and D^{**}. To determine the B decay branching ratios, we assumed $\mathcal{B}[D^{**0}(2420) \to D^{*+}\pi^-]$ and $\mathcal{B}[D^{**0}(2460) \to D^{*+}\pi^-]$ are 67% and 20% respectively. We also assume that $\mathcal{B}[D^{**0}(2460) \to D^+\pi^-]$ and $\mathcal{B}[D^{***+}(2460) \to D^0\pi^+]$ are 30% and 30% respectively.

decays. It is also possible to use the $\bar{B}^0 \to \psi K^{*0}$ decay (where $K^{*0} \to K^0_S\pi^0$) to measure this CP asymmetry. However, this final state has even CP if the orbital angular momentum L, between the ψ and K^{*0}, is 0 or 2, and CP is odd for $L = 1$. If both CP states are present the CP asymmetry will be diluted. A measurement of CP violation in this channel may be possible if one of the CP states dominates, or if a detailed moments analysis of the various decay components is performed [33]. We present a measurement of the polarization in the decay $\bar{B}^0 \to \psi K^{*0}$ which allows us to determine the fractions of the two CP states.

B. Branching ratios

B meson candidates are formed by combining a charmonium and a strange meson candidate. We reconstruct K^0_S decays into $\pi^+\pi^-$ pairs which have vertices displaced from the beam axis by greater than 5 mm. Only the $K^+\pi^-$ channel is used to form K^{*0} mesons while K^{*-} candidates are reconstructed in the decay channels $K^0_S\pi^-$ and $K^-\pi^0$. The $K\pi$ invariant mass must be within ± 75 MeV of the nominal K^* mass. In the $B^- \to \psi K^{*-}$, $K^{*-} \to K^-\pi^0$ mode, only the half of the K^{*-} helicity angle distribution with a fast π^0 is used. The ψ and ψ' candidates decaying into lepton pairs were kinematically

TABLE VIII. Branching ratio for $B \to D^{**}(n\pi)$.

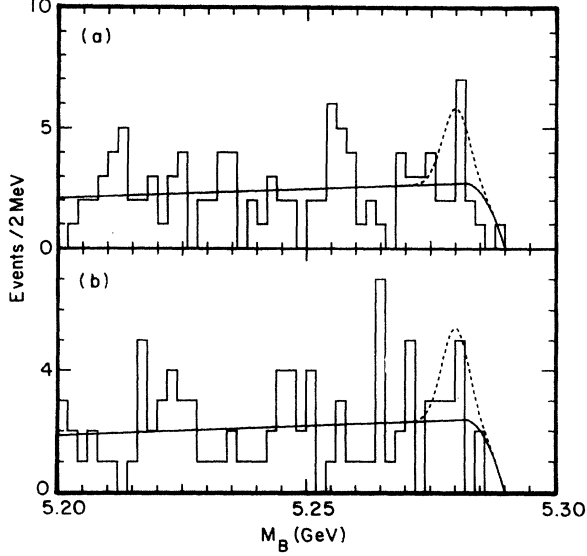| Mode	CLEO II	Bari model [31]	RI model [32]
$D^{**0}(2420)\pi^-$	$(11 \pm 5 \pm 2 \pm 1) \times 10^{-4}$	4×10^{-4}	$7.5 \times 10^{-4} - 13 \times 10^{-4}$
$D^{**0}(2460)\pi^-$ ($D^{**0} \to D^{*+}\pi^-$)	$< 2.8 \times 10^{-3}$	6×10^{-4}	$5 \times 10^{-4} - 8 \times 10^{-4}$
$D^{**0}(2460)\pi^-$ ($D^{**0} \to D^+\pi^-$)	$< 1.3 \times 10^{-3}$	6×10^{-4}	$5 \times 10^{-4} - 8 \times 10^{-4}$
$D^{**+}(2460)\pi^-$ ($D^{**+} \to D^0\pi^+$)	$< 2.2 \times 10^{-3}$	6×10^{-4}	$5 \times 10^{-4} - 8 \times 10^{-4}$
$D^{**0}(2420)\rho^-$	$< 1.4 \times 10^{-3}$	1×10^{-3}	$13 \times 10^{-4} - 24 \times 10^{-4}$
$D^{**0}(2460)\rho^-$	$< 5 \times 10^{-3}$	1×10^{-3}	$10 \times 10^{-4} - 20 \times 10^{-4}$

FIG. 20. Beam-constrained mass distributions for (a) $B^- \to D^+\pi^-\pi^-$ and (b) $\bar{B}^0 \to D^0\pi^-\pi^+$. The curve is the result of the fit and the dotted line is the 90% confidence level upper limit.

constrained to the known mass values in order to improve the resolution on ΔE. Using the procedures described in Sec. III we reconstruct B meson candidates and obtain the beam constrained mass distributions shown in Figs. 22, 23, and 24. The corresponding branching ratios are listed in Table IX.

The systematic errors in the branching ratio measurements include contributions from number of B mesons (2.5%), tracking efficiencies (2% per charged track), π^0 detection efficiency (5%), dE/dx efficiency (2% per identified track), lepton detection efficiency (2% per lepton), Monte Carlo statistics (1.5–6%), the ψ leptonic branching ratio (4.2%), and the branching ratios for ψ' and χ_{c1} decays.
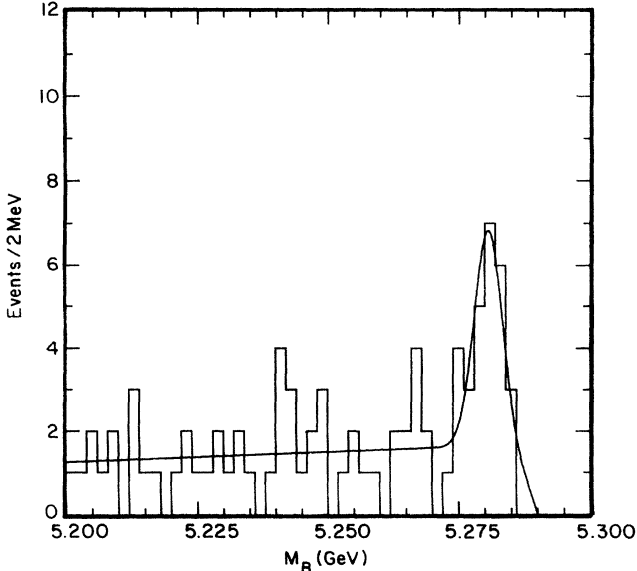
The results for the B^- and B^0 decay modes can be

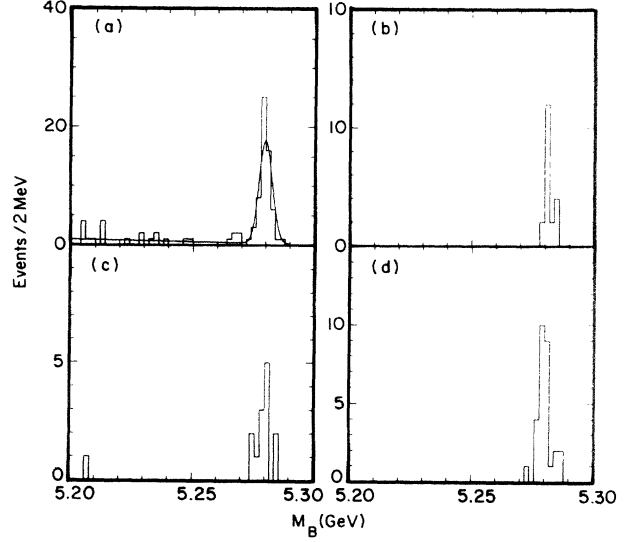FIG. 21. Beam-constrained mass distribution for $B^- \to D^{*+}\pi^-\pi^-$.

FIG. 22. Beam-constrained mass for (a) $B^- \to \psi K^-$, (b) $\bar{B}^0 \to \psi \bar{K}^0$, (c) $B^- \to \psi \bar{K}^{*-}$, and (d) $\bar{B}^0 \to \psi K^{*0}$.

combined using isospin symmetry to determine the vector to pseudoscalar production ratio

$$\frac{\mathcal{B}(B \to \psi K^*)}{\mathcal{B}(B \to \psi K)} = 1.71. \tag{10}$$

The revised [8] Bauer-Stech-Wirbel (BSW) model [34] predicts a value of 1.61 for this quantity. This model uses the ratio of $B \to K^*/B \to K$ form factors determined from harmonic oscillator wave functions and assumes that the factorization hypothesis is valid for internal spectator decays.

C. Polarization in ψK^*

After integration over the azimuthal angle between the ψ and the K^* decay planes, the angular distribution in $B \to \psi K^*$ decays can be written as [27]
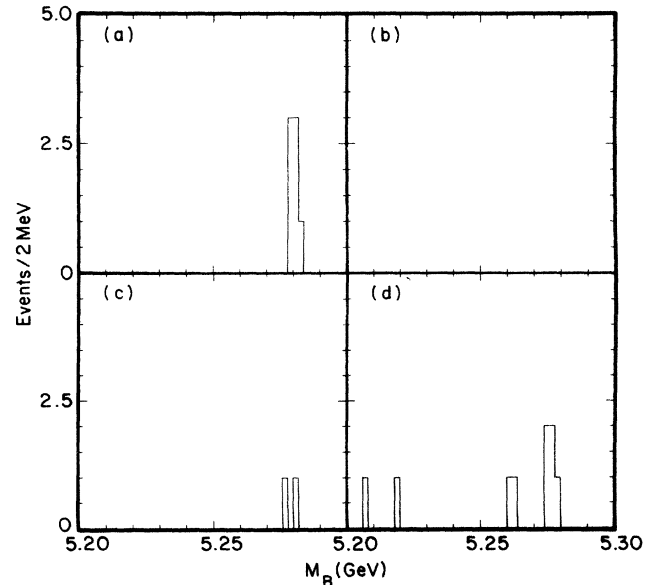

FIG. 23. Beam-constrained mass for (a) $B^- \to \psi' K^-$, (b) $\bar{B}^0 \to \psi' \bar{K}^0$, (c) $B^- \to \psi' \bar{K}^{*-}$, and (d) $\bar{B}^0 \to \psi' K^{*0}$.

TABLE IX. Exclusive $B \to c\bar{c}$ branching ratios and 90% confidence level upper limits (%).

B mode	$\sigma(\Delta E)$	No. of events	ϵ [a]	B (%)
$B^- \to \psi K^-$	13	58.7 ± 7.9	0.47	$0.110 \pm 0.015 \pm 0.009$
$B^0 \to \psi K^0$	13	10.0 ± 3.2	0.34	$0.075 \pm 0.024 \pm 0.008$
$B^0 \to \psi K^{*0}$	12	29.0 ± 5.4	0.23	$0.169 \pm 0.031 \pm 0.018$
$B^- \to \psi K^{*-}, K^{*-} \to K^- \pi^0$	21	6.0 ± 2.4	0.07	$0.218 \pm 0.089 \pm 0.026$
$B^- \to \psi K^{*-}, K^{*-} \to K_S^0 \pi^-$	11	6.6 ± 2.7	0.17	$0.130 \pm 0.058 \pm 0.018$
$B^- \to \psi K^{*-}$ (combined)		12.6 ± 3.6		$0.178 \pm 0.051 \pm 0.023$
$B^- \to \psi' K^-$	9.8, 11	7.0 ± 2.6	0.36, 0.15	$0.061 \pm 0.023 \pm 0.009$
$B^0 \to \psi' K^0$	8.4, 10	0	0.28, 0.11	< 0.08
$B^0 \to \psi' K^{*0}$	9.7, 10	4.2 ± 2.3	0.24, 0.091	< 0.19
$B^- \to \psi' K^{*-}, K^{*-} \to K^- \pi^0$	18, 17	1 ± 1	0.077, 0.023	< 0.56
$B^- \to \psi' K^{*-}, K^{*-} \to K_S^0 \pi^-$	7.9, 9.8	1 ± 1	0.16, 0.057	< 0.36
$B^- \to \psi' K^{*-}$ (combined)		2 ± 1.4		< 0.30
$B^- \to \chi_{c1} K^-$	18	6 ± 2.4	0.20	$0.097 \pm 0.040 \pm 0.009$
$B^0 \to \chi_{c1} K^0$	16	1 ± 1	0.14	< 0.27
$B^0 \to \chi_{c1} K^{*0}$	15	1.2 ± 1.5	0.13	< 0.21
$B^- \to \chi_{c1} K^{*-}, K^{*-} \to K^- \pi^0$	15	0	0.033	< 0.67
$B^- \to \chi_{c1} K^{*-}, K^{*-} \to K_s \pi^-$	17	0	0.11	< 0.30
$B^- \to \chi_{c1} K^{*-}$ (combined)		0		< 0.21

[a]This efficiency does not include the ψ, ψ', χ_{c1}, K^0, K^*, or K_S^0 branching ratios. The two sets of values given for the ψ' channels correspond to the two ψ' decay modes $\psi' \to l^+ l^-$ and $\psi' \to \psi \pi^+ \pi^-$.

$$\frac{d^2\Gamma}{d\cos\Theta_\psi d\cos\Theta_{K^*}} \propto \frac{1}{4}\sin^2\Theta_{K^*}(1 + \cos^2\Theta_\psi)(|H_{+1}|^2 + |H_{-1}|^2) + \cos^2\Theta_{K^*}\sin^2\Theta_\psi|H_0|^2, \tag{11}$$

where the K^* helicity angle Θ_{K^*} is the angle between the kaon direction in the K^* rest frame and the K^* direction in the B rest frame, Θ_ψ is the corresponding ψ helicity angle, and the $H_{\pm 1, 0}$ are the helicity amplitudes.

There are 29 $\bar{B}^0 \to \psi K^{*0}$ candidates and 13 $B^- \to \psi K^{*-}$ candidates. After correcting for detector acceptance, we perform an unbinned maximum likelihood fit

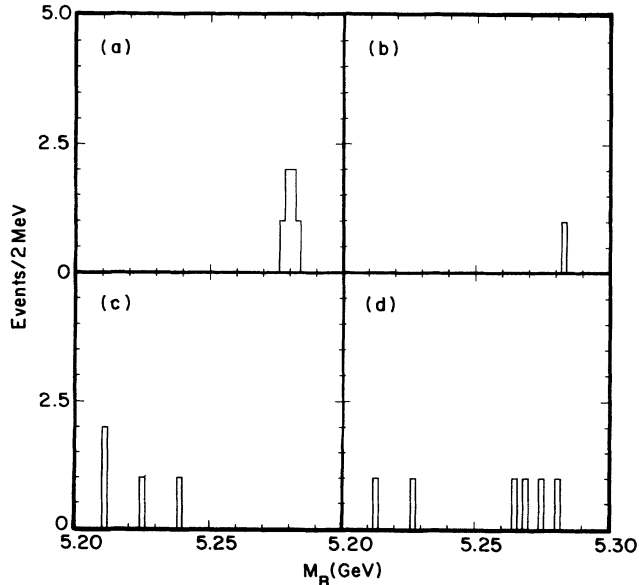FIG. 24. Beam-constrained mass for (a) $B^- \to \chi_{c1} K^-$, (b) $\bar{B}^0 \to \chi_{c1} \bar{K}^0$, (c) $B^- \to \chi_{c1} K^{*-}$, and (d)$\bar{B}^0 \to \chi_{c1} \bar{K}^{*0}$.

to the double differential distribution described in the equation above. The fit gives the fraction of longitudinal polarization in $B \to \psi K^*$ as

$$\left(\frac{\Gamma_L}{\Gamma}\right)_{B \to \psi K^*} = 0.80 \pm 0.08 \pm 0.05. \tag{12}$$

The systematic error in this measurement is dominated by the uncertainty in the acceptance. The efficiency corrected distributions for each of the helicity angles $\cos\Theta_\psi$ and $\cos\Theta_{K^*}$ are shown in Fig. 25.

This result can be compared to the theoretical predictions of Kramer and Palmer [35] which depends on the unmeasured $B \to K^*$ form factor. Using the BSW model to estimate the form factor, they find $\Gamma_L/\Gamma = 0.57$. Using heavy quark effective theory (HQET) and experimental measurements of the $D \to K^*$ form factor, they obtain $\Gamma_L/\Gamma = 0.73$.

The decay mode $B \to \psi K^*$ may not be completely polarized, but it is dominated by a single CP eigenstate ($CP = -1$ produced with $L = 1$). This mode will therefore be useful for measurements of CP violation.

VIII. SEARCH FOR COLOR SUPPRESSED DECAYS

We search for B decays that can occur via an internal W-emission graph, but which do not lead to final states with charmonium [36]. One expects that these decays will be suppressed relative to decays which occur via the
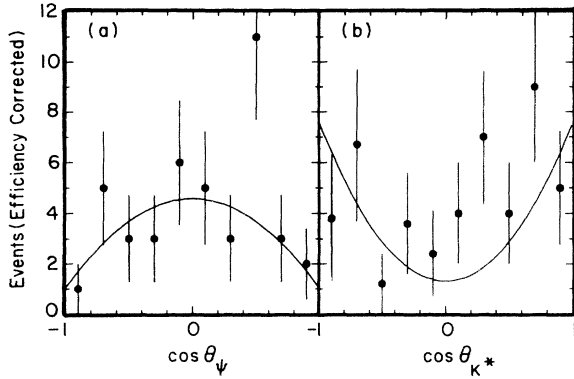
M. S. ALAM *et al.*

FIG. 25. Distribution of (a) the ψ and (b) the K^* efficiency corrected helicity distributions in $B \to \psi K^*$ decays. The overlaid curves are projections of the unbinned maximum likelihood fit described in the text.

external W-emission graph. For the internal graph the colors of the quarks from the virtual W must match the colors of the c quark and the accompanying spectator antiquark. In a simple picture, one expects that the suppression factor should be about 1/18 for decays involving π^0, ρ^0, and ω mesons [37], but in heavy quark decays the effects of gluons cannot be neglected. These decays can be used to test QCD based calculations [8] which predict suppression factors of order 1/50. If color-suppressed B decay modes are not greatly suppressed then these modes could be useful for CP violation studies [38].

We search for color-suppressed decay modes of B mesons which contain a single D meson (or D^* meson) in the final state. The relevant color-suppressed modes are given in Table X. We use the decay modes $\eta \to \gamma\gamma$, $\omega \to \pi^+\pi^-\pi^0$ and $\eta' \to \eta\pi^+\pi^-$, followed by $\eta \to \gamma\gamma$ [39].

For decays of a pseudoscalar meson into a final state containing a pseudoscalar and a vector meson, a helicity angle cut of $|\cos\Theta_V| > 0.4$ is used [40]. No convincing signals were found in the decay modes that were examined. Upper limits on the branching ratios for color-suppressed modes are given in Table X. The 90% confidence level upper limits are calculated using the prescription described by the PDG [41]. These upper limits take into account the systematic uncertainty in the back-

TABLE X. Upper limits (UL's) (90% C.L.) on branching fractions for color suppressed B decays.

Decay mode	Events	ϵ[a]	UL (%) at 90% C.L.
$\bar{B}^0 \to D^0\pi^0$	< 20.7	$0.32, 0.16, 0.18$	< 0.048
$\bar{B}^0 \to D^0\rho^0$	< 19.0	$0.21, 0.08, 0.12$	< 0.055
$\bar{B}^0 \to D^0\eta$	< 9.5	$0.31, 0.11, 0.16$	< 0.068
$\bar{B}^0 \to D^0\eta'$	< 3.5	$0.18, 0.08, 0.11$	< 0.086
$\bar{B}^0 \to D^0\omega$	< 12.7	$0.16, 0.07, 0.09$	< 0.063
$\bar{B}^0 \to D^{*0}\pi^0$	< 11.0	$0.13, 0.07, 0.07$	< 0.097
$\bar{B}^0 \to D^{*0}\rho^0$	< 8.1	$0.09, 0.04, 0.04$	< 0.117
$\bar{B}^0 \to D^{*0}\eta$	< 2.3	$0.11, 0.05, 0.06$	< 0.069
$\bar{B}^0 \to D^{*0}\eta'$	< 2.3	$0.07, 0.03, 0.03$	< 0.27
$\bar{B}^0 \to D^{*0}\omega$	< 9.0	$0.06, 0.03, 0.03$	< 0.21

[a]The efficiencies for the $D^0 \to K^-\pi^+$, $D^0 \to K^-\pi^+\pi^0$, and $D^0 \to K^-\pi^+\pi^-\pi^+$ modes are given. These efficiencies do not include D, D^* η, η', and ω branching ratios.
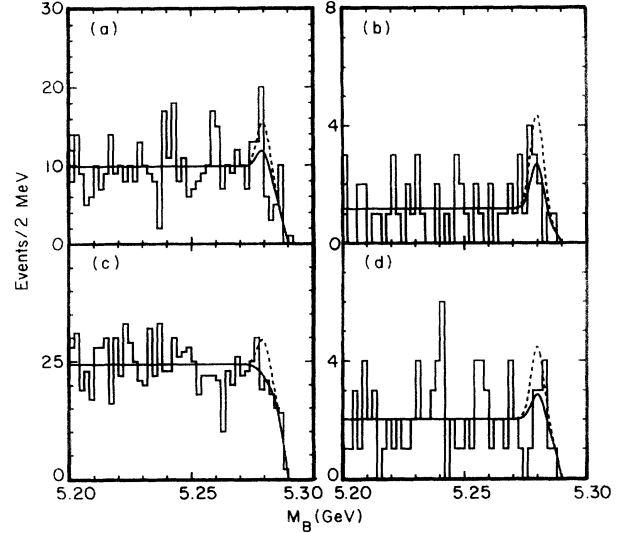

FIG. 26. Beam-constrained mass distributions for (a) $\bar{B}^0 \to D^0\pi^0$, (b) $\bar{B}^0 \to D^{*0}\pi^0$, (c) $\bar{B}^0 \to D^0\rho^0$, and (d) $\bar{B}^0 \to D^{*0}\rho^0$. The curves are the results of a fit with the CLEO background shape. The dotted lines show the 90% C.L. upper limit.

ground level as well as the systematic uncertainty in the detection efficiency. In Figs. 26, 27, and 28 we show the fitted distributions for the color-suppressed modes with the fit superimposed on each plot. Upper limits on the ratios of color-suppressed modes to normalization modes are given in Table XI.

IX. THE $B^- - \bar{B}^0$ MASS DIFFERENCE

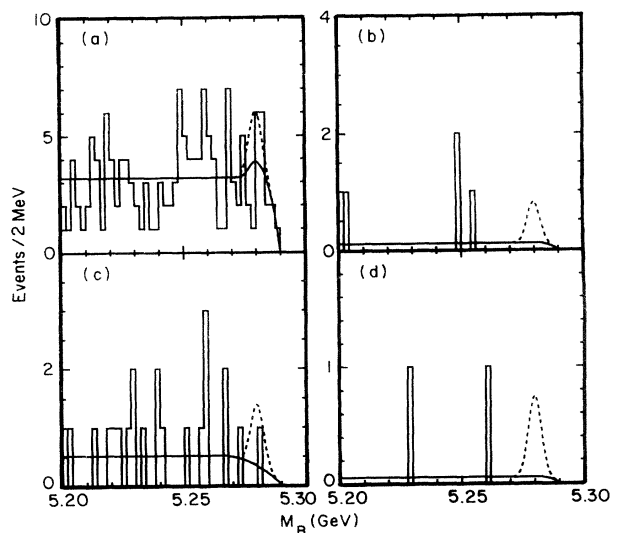We now proceed to measurements of the $\bar{B}^0$ and B^- masses and the mass difference between them. For this

FIG. 27. Beam-constrained mass distributions for (a) $\bar{B}^0 \to D^0\eta$, (b) $\bar{B}^0 \to D^{*0}\eta$, (c) $\bar{B}^0 \to D^0\eta'$, and (d) $\bar{B}^0 \to D^{*0}\eta'$. The curves are the results of a fit with the CLEO background shape. The dotted lines show the 90% C.L. upper limit.
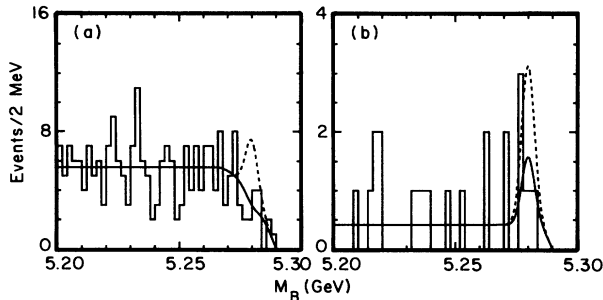
FIG. 28. Beam-constrained mass distributions for (a) $\bar{B}^0 \to D^0\omega$ and (b) $\bar{B}^0 \to D^{*0}\omega$. The curves are the results of the fit. The dotted lines show the 90% C.L. upper limit.

analysis we use the decays $B^- \to \psi K^-$, $\bar{B}^0 \to \psi K^{*0}$, $B^- \to D^0\pi^-$, $B^- \to D^0\rho^-$, $B^- \to D^{*0}\pi^-$, $B^- \to D^{*0}\rho^-$, $\bar{B}^0 \to D^+\pi^-$, $\bar{B}^0 \to D^+\rho^-$, $\bar{B}^0 \to D^{*+}\pi^-$, and $\bar{B}^0 \to D^{*+}\rho^-$ for which the signal-to-background ratio is large. For the decays $B^- \to D^0\pi^-$ and $B^- \to D^0\rho^-$ only the $D^0 \to K^-\pi^+$ mode is used. The M_B distributions for the sum of these modes are shown in Fig. 29. We have a total of 362 B^- and 340 $\bar{B}^0$ signal events. The data are fitted with a Gaussian of fixed width (2.7 MeV) determined by Monte Carlo simulation. The width is assumed to be the same for all modes. The fitted masses for each mode and their statistical errors are given in Table XII. We apply a correction for initial state radiation as described in Ref. [42], of magnitude -1.1 ± 0.5 MeV, to arrive at the final values for the B^- and $\bar{B}^0$ masses of $5278.8 \pm 0.2 \pm 0.5 \pm 2.0$ MeV and $5279.2 \pm 0.2 \pm 0.5 \pm 2.0$ MeV, respectively. The first systematic error results from the uncertainty in the initial state radiation correction. The second systematic error is due to the uncertainty in the absolute value of the CESR energy scale, which is determined by calibrating to the known $\Upsilon(1S)$ mass [43].

The mass difference is determined to be $0.41 \pm 0.25 \pm 0.19$ MeV. This is more accurate than the masses themselves because the beam energy uncertainty cancels, as do many systematic errors associated with the measurement errors on the charged tracks and π^0 mesons. The remaining systematic error is found by making a number of tests of the stability of our result.

A systematic shift of 0.12 MeV is produced by using different background shapes for the B^- and $\bar{B}^0$ modes [44]. We have also investigated the effect of changing the

TABLE XI. Upper limits on ratios of branching ratios for color suppressed to normalization modes.

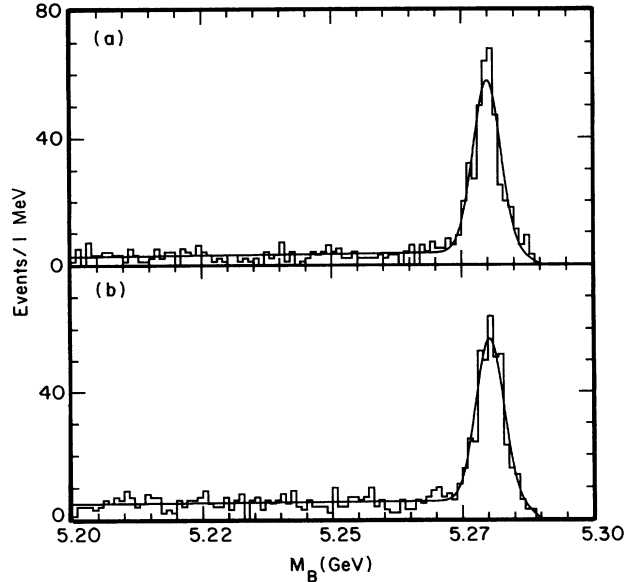| Ratio of branching ratios	UL (90% C.L.)
$\mathcal{B}(\bar{B}^0 \to D^0\pi^0)/\mathcal{B}(B^- \to D^0\pi^-)$	< 0.09
$\mathcal{B}(\bar{B}^0 \to D^0\rho^0)/\mathcal{B}(B^- \to D^0\rho^-)$	< 0.05
$\mathcal{B}(\bar{B}^0 \to D^0\eta)/\mathcal{B}(B^- \to D^0\pi^-)$	< 0.12
$\mathcal{B}(\bar{B}^0 \to D^0\eta')/\mathcal{B}(B^- \to D^0\pi^-)$	< 0.16
$\mathcal{B}(\bar{B}^0 \to D^0\omega)/\mathcal{B}(B^- \to D^0\rho^-)$	< 0.05
$\mathcal{B}(\bar{B}^0 \to D^{*0}\pi^0)/\mathcal{B}(B^- \to D^{*0}\pi^-)$	< 0.20
$\mathcal{B}(\bar{B}^0 \to D^{*0}\rho^0)/\mathcal{B}(B^- \to D^{*0}\rho^-)$	< 0.07
$\mathcal{B}(\bar{B}^0 \to D^{*0}\eta)/\mathcal{B}(B^- \to D^{*0}\pi^-)$	< 0.14
$\mathcal{B}(\bar{B}^0 \to D^{*0}\eta')/\mathcal{B}(B^- \to D^{*0}\pi^-)$	< 0.54
$\mathcal{B}(\bar{B}^0 \to D^{*0}\omega)/\mathcal{B}(B^- \to D^{*0}\rho^-)$	< 0.09

FIG. 29. M_B for (a) B^- events and (b) $\bar{B}^0$ events.

photon energy calibration. A change of 0.5%, the quoted systematic error, results in a 0.15 MeV change in the fitted B mass in both the $D^{*+}\rho^-$ and $D^{*0}\rho^-$ final states. This effect almost completely cancels in the mass difference measurement where it contributes an error of <0.03 MeV. This is because the shift of the π^0 energy in the ρ^- cancels in the difference leaving only the shift of the energy of the slow π^0 from the D^{*0} which is uncorrelated with the direction of the B meson. A similar test where we scale the measured momentum of the slow pion from the D^{*+} by 5% also does not affect the mass difference for the same reason.

We have also checked the stability of the result with changes in event samples. For example, we have used only half of the $\cos\Theta_\rho$ distributions in $B \to D^{(*)}\rho$ modes and we have used less stringent lepton identification criteria for the $B \to \psi K^-$ mode. We estimate a systematic of 0.15 MeV from these studies.

The different sources of systematic errors are listed in Table XIII and are combined in quadrature. We compare our result with previous results in Table XIV.

There are several models which predict the isospin mass difference to be between 1.2 and 2.3 MeV which are larger than the value reported here [45]. However, Goity and Hou (-0.5 ± 0.6 MeV) and Lebed (0.89 MeV) can

TABLE XII. B masses from individual modes (not corrected for initial state radiation).

	B^- modes			$\bar{B}^0$ modes	
Mode	Mass (MeV)	Events	Mode	Mass (MeV)	Events
$D^{*0}\pi^-$	5279.7±0.4	73	$D^{*+}\pi^-$	5280.1±0.4	73
$D^{*0}\rho^-$	5280.2±0.4	89	$D^{*+}\rho^-$	5280.5±0.4	79
ψK^-	5279.8±0.4	44	ψK^{*0}	5280.4±0.5	29
$D^0\pi^-$	5279.9±0.3	76	$D^+\pi^-$	5280.4±0.3	80
$D^0\rho^-$	5279.7±0.4	80	$D^+\rho^-$	5280.3±0.4	79
All	5279.9±0.2	362	All	5280.3±0.2	340

TABLE XIII. Contributions to the systematic error in the $B^0 - B^-$ mass difference.

Event sample	0.15 MeV
Background shape	0.12 MeV
γ energy calibration	< 0.03 MeV
Width of B mass peak	< 0.02 MeV
Track momentum scale	< 0.01 MeV
Total	0.19 MeV

accommodate this small mass difference in their models [46].

X. TESTS OF THE FACTORIZATION HYPOTHESIS

A. Introduction

Our large data sample has made possible the precise branching ratio and polarization measurements discussed above. In the following sections we address many important questions about nonleptonic B meson decay.

By comparing rates and polarizations of semileptonic and hadronic decays we can perform tests of the factorization hypothesis, which is the basis of most theoretical treatment of hadronic B decays. In analogy with semileptonic decays, where the amplitude factorizes into the product of a leptonic and hadronic current since leptons are not sensitive to the strong interaction, it is possible that two-body decays of B mesons which occur via the external spectator process may be expressed theoretically as the product of two independent hadronic currents, one describing the formation of a charm meson and the other the hadronization of the $\bar{u}d$ (or $\bar{c}s$) system from the virtual W^-.

There are few models of hadronic B decays. Those which exist predict widths of two-body decays and assume the validity of the factorization hypothesis. Although factorization fails in many D decays [47], it is hoped that factorization will be a better approximation in B decays due to the larger energy release present [48].

If factorization is valid, then heavy quark effective theory, henceforth referred to as HQET [49], could provide a reliable, model-independent framework for the calculation of properties of nonleptonic B meson decays. In addition, if factorization holds, then measurements of nonleptonic B decays may be used to extract fundamental parameters of the standard model. For instance the CKM matrix element V_{ub} can be determined from $B^0 \to \pi^+\pi^-$

TABLE XIV. Measurements of the $\bar{B}^0$-B^- mass difference.

Experiment	$M(\bar{B}^0)$-$M(B^-)$ (MeV)
CLEO 87 [2]	$2.0 \pm 1.1 \pm 0.3$
ARGUS [6]	$-0.9 \pm 1.2 \pm 0.5$
CLEO 92 [3]	$-0.4 \pm 0.6 \pm 0.5$
CLEO 93 (this result)	$0.41 \pm 0.25 \pm 0.19$
Average	0.4 ± 0.3

or $\bar{B}^0 \to D_s^-\pi^+$, and the decay constant f_{D_s} can be determined from $\bar{B}^0 \to D_s^-D^{*+}$.

B. Branching ratio tests

Assuming factorization, the effective Hamiltonian Eq. (2) for a nonleptonic B decay can be written as a product of two hadronic currents. Consider the case of $\bar{B}^0 \to D^{*+}h^-$, where h is a hadron. The amplitude for this reaction is

$$A = (G_F/\sqrt{2})\ V_{cb}V_{ud}^*\langle h^-(p)|(\bar{d}u)|0\rangle\langle D^{*+}|(\bar{c}b)|\bar{B}^0\rangle \quad (13)$$

where V_{ud} is the well-measured CKM factor from the $W^- \to \bar{u}d$ vertex. The first hadron current, which creates the h^- from the vacuum, is related to the decay constant f_h, and is known for $h = \pi, \rho$. We have

$$\langle h^-(p)|(\bar{d}u)|0\rangle = -if_hp_\mu, \quad (14)$$

where p_μ is the h^- four-momentum. The other hadron current can be found from semileptonic $\bar{B}^0 \to D^{*+}\ell^-\bar{\nu}_\ell$ decays. Here the amplitude is the product of a lepton current and the hadron current that we seek to insert in Eq. (13). Factorization can be tested experimentally by verifying whether the relation

$$\frac{\Gamma\left(\bar{B}^0 \to D^{*+}h^-\right)}{\left.\dfrac{d\Gamma}{dq^2}\left(\bar{B}^0 \to D^{*+}l^-\bar{\nu}_l\right)\right|_{q^2=m_h^2}} = 6\pi^2 c_1^2 f_h^2|V_{ud}|^2 \quad (15)$$

is satisfied, where q^2 is the four-momentum transfer from the B meson to the D^* meson. Since q^2 is also the mass of the lepton-neutrino system, by setting $q^2 = m_h^2$ we are simply requiring that the lepton-neutrino system has the same kinematic properties as the h^- in the hadronic decay. The c_1^2 term accounts for hard gluon corrections. Here we use $c_1 = 1.1 \pm 0.1$ as deduced from perturbative QCD. The error in c_1 reflects the uncertainty in the mass scale at which the coefficent c_1 should be evaluated [50]. For the case where $h^- = \pi^-$ and $c_1=1$, Eq. (15) was found to be satisfied by Bortoletto and Stone [51]. In the following the left-hand side of Eq. (15) will be denoted $R_{\rm expt}$ and the right-hand side will be denoted $R_{\rm theo}$.

This type of factorization test can also be performed using $\bar{B}^0 \to D^{*+}h^-$ decays where $h^- = \rho^-$ or $a_1(1260)^-$. For the ρ^- case, the decay constant can be determined from $e^+e^- \to \rho^0$ or from τ decays. The first method leads to $f_\rho = 215 \pm 4$ MeV. Taking into account the ρ width, Pham and Vu [52] find that $\Gamma(\tau^- \to \nu\rho^-) = 0.804(G_F^2/16\pi)\ |V_{ud}^2|M_\tau^3 f_\rho^2$ which gives $f_\rho = 212.0 \pm 5.3$ MeV [53]. We take the first value. We also perform this test for $\bar{B}^0 \to D^{*+}a_1^-$ where we use $f_{a_1} = 205 \pm 16$ MeV [32]. To derive numerical predictions for branching ratios, we must interpolate the observed differential q^2 distribution [54] for $\bar{B} \to D^*\ell\ \nu$ to $q^2 = m_\pi^2$, m_ρ^2, and $m_{a_1}^2$, respectively. Until this distribution is measured more precisely theoretical models must be used for the slope of the distribution. Thus the results are stated below for different models. For-

tunately, the spread in the theoretical models which describe $\bar{B} \to D^*\ell\,\nu$ is small (see Fig. 30).

We now have all the required ingredients [55] for the test with decay rates (see Table XV). Using the extrapolation of the q^2 spectrum [56] from the BSW model as the central value, we obtain from Eq. (15) the results given in Table XVI.

If we form ratios of branching fractions some of the systematic uncertainties on R_{expt} will cancel, as does the QCD correction c_1 in R_{theor}. For example in the case of $D^{*+}\rho^-/D^{*+}\pi^-$, the expectation from factorization is given by $R_{\mathrm{theor}}(\rho)/R_{\mathrm{theor}}(\pi)$ times the ratio of the semileptonic branching ratios evaluated at the appropriate q^2 values. In Table XVII we show the comparison of the data, the expectation from factorization as defined above, and two theoretical predictions of BSW [34] and Reader and Isgur (RI) [32].

From the measurements described above, we find that at the present level of precision, there is agreement between experiment and the expectation from factorization for the q^2 range: $0 < q^2 < m_{a_1}^2$.

C. Factorization and angular correlations

More subtle tests of the factorization hypothesis can be performed by examining the polarization in B meson decays into two vector mesons. This idea was suggested by Körner and Goldstein [57]. Again, the underlying principle is that hadronic decays are analogous to the appropriate semileptonic decays evaluated at a fixed value of q^2. For instance, the ratio of longitudinal to transverse polarization (Γ_L/Γ_T) in $\bar{B}^0 \to D^{*+}\rho^-$ should be equal to the corresponding ratio for $B \to D^*l^-\bar{\nu}$ evaluated at $q^2 = m_\rho{}^2 = 0.6$ GeV^2:
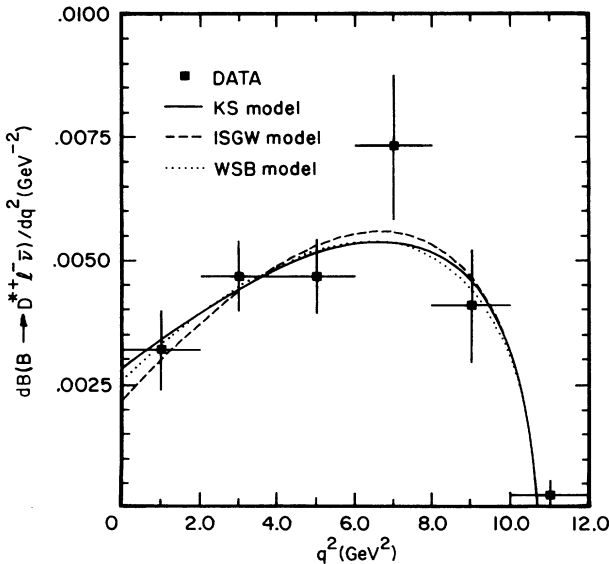

FIG. 30. The Q^2 distribution for the decay $\bar{B}^0 \to D^{*+}\ell^-\bar{\nu}_\ell$. This is a weighted average from CLEO and ARGUS data. The curves are fits using various models of semileptonic decays (from Ref. [51]).

TABLE XV. Ingredients for factorization tests.

$|c_1|$	1.12 ± 0.10
f_π	131.74 ± 0.15 MeV
f_ρ	215 ± 4 MeV
f_{a_1}	205 ± 16 MeV
V_{ud}	0.975 ± 0.001
$d\mathcal{B}(B \to D^*l\,\nu)/dq^2|_{q^2=m_\pi^2}$ (BSW)	0.0023 GeV^{-2}
$d\mathcal{B}(B \to D^*l\,\nu)/dq^2|_{q^2=m_\pi^2}$ (ISGW)	0.0020 GeV^{-2}
$d\mathcal{B}(B \to D^*l\,\nu)/dq^2|_{q^2=m_\pi^2}$ (KS)	0.0024 GeV^{-2}
$d\mathcal{B}(B \to D^*l\,\nu)/dq^2|_{q^2=m_\rho^2}$ (BSW)	0.0025 GeV^{-2}
$d\mathcal{B}(B \to D^*l\,\nu)/dq^2|_{q^2=m_\rho^2}$ (ISGW)	0.0024 GeV^{-2}
$d\mathcal{B}(B \to D^*l\,\nu)/dq^2|_{q^2=m_\rho^2}$ (KS)	0.0027 GeV^{-2}
$d\mathcal{B}(B \to D^*l\,\nu)/dq^2|_{q^2=m_{a_1}^2}$ (BSW)	0.0032 GeV^{-2}
$d\mathcal{B}(B \to D^*l\,\nu)/dq^2|_{q^2=m_{a_1}^2}$ (ISGW)	0.0030 GeV^{-2}
$d\mathcal{B}(B \to D^*l\,\nu)/dq^2|_{q^2=m_{a_1}^2}$ (KS)	0.0033 GeV^{-2}

$$\frac{\Gamma_L}{\Gamma_T}(\bar{B}^0 \to D^{*+}\rho^-) = \frac{\Gamma_L}{\Gamma_T}(B \to D^*l^-\bar{\nu}_L)|_{q^2=m_\rho^2}. \quad (16)$$

The advantage of this method is that it is not affected by QCD corrections [58].

For $B \to D^*\,l\,\nu$ decay, longitudinal polarization dominates at low q^2. Near $q^2 = q^2_{\mathrm{max}}$, by contrast, transverse polarization dominates. There is a simple physical argument for the behavior of the form factors near these two kinematic limits. Near $q^2 = q^2_{\mathrm{max}}$, the D^* is almost at rest. Its small velocity is uncorrelated with the D^* spin, so all three possible D^* helicities are equally likely. As $q^2 \to q^2_{\mathrm{max}}$ we expect $\Gamma_T/\Gamma_L = 2$. At $q^2 = 0$, the D^* has the maximum possible momentum, while the lepton and neutrino are collinear and travel in the direction opposite to the D^* with their helicities aligned to give $S_z = 0$. Thus, near $q^2 = 0$ longitudinal polarization is dominant.

For $\bar{B}^0 \to D^{*+}\rho^-$, Rosner predicts 88% longitudinal polarization from the argument described above [59]. Similar results can be extracted from the work of Neubert [60] and Kramer *et al.* [61]. Figure 31 shows Neubert's result for the production of transversely and longitudinally polarized D^* mesons in $B \to D^*\,l\,\nu$ decays. Using this figure we find Γ_L/Γ to be approximately 85% for $q^2 = m_\rho{}^2 = 0.6$, which agrees well with Rosner's prediction [59].

The agreement between these predictions and the experimental result (see Sec. V B)

$$\Gamma_L/\Gamma = (93 \pm 5 \pm 5)\% \quad (17)$$

supports the factorization hypothesis in hadronic B meson decay for q^2 values up to m_ρ^2.

TABLE XVI. Comparison of R_{expt} and R_{theor}.

	R_{expt} (GeV^2)	R_{theor} (GeV^2)
$\bar{B}^0 \to D^{*+}\pi^-$	$1.1 \pm 0.1 \pm 0.2$	1.2 ± 0.2
$\bar{B}^0 \to D^{*+}\rho^-$	$3.0 \pm 0.4 \pm 0.6$	3.3 ± 0.5
$\bar{B}^0 \to D^{*+}a_1^-$	$4.0 \pm 0.6 \pm 0.5$	3.0 ± 0.5

M. S. ALAM *et al.*

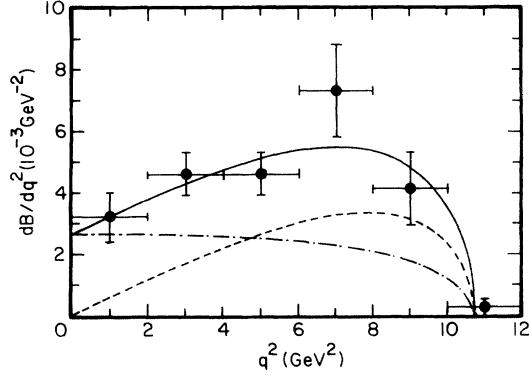FIG. 31. The differential branching ratio for $\bar{B}^0 \to D^{*+}\ell\bar{\nu}_\ell$. The curves show the theoretical prediction for producing transversely (dashed) and longitudinally (dash-dotted) polarized D^* mesons, as well as the total decay rate (solid) (from Ref. [60]).

XI. TESTS OF SPIN SYMMETRY IN HQET

If the factorization hypothesis holds, then certain hadronic B meson decay modes can be used to test the spin symmetry of HQET. In this theory the effect of the heavy quark magnetic moment does not enter to lowest order [62] , so it is expected that

$$\Gamma(\bar{B}^0 \to D^+\pi^-) = \Gamma(\bar{B}^0 \to D^{*+}\pi^-) \tag{18}$$

and

$$\Gamma(\bar{B}^0 \to D^+\rho^-) = \Gamma(\bar{B}^0 \to D^{*+}\rho^-). \tag{19}$$

After correcting for phase space and deviations from heavy quark symmetry, one expects that $\mathcal{B}(\bar{B}^0 \to D^+\pi^-) = 1.03\, \mathcal{B}(\bar{B}^0 \to D^{*+}\pi^-)$ and $\mathcal{B}(\bar{B}^0 \to D^+\rho^-) = 0.89\, \mathcal{B}(\bar{B}^0 \to D^{*+}\rho^-)$. A separate calculation by Blok and Shifman [63] using a QCD sum rule approach predicts that $\mathcal{B}(\bar{B}^0 \to D^+\pi^-) = 1.2\, \mathcal{B}(\bar{B}^0 \to D^{*+}\pi^-)$ due to the presence of nonfactorizable contributions. From our data we find

$$\frac{\mathcal{B}(\bar{B}^0 \to D^+\pi^-)}{\mathcal{B}(\bar{B}^0 \to D^{*+}\pi^-)} = 1.12 \pm 0.19 \pm 0.24 \tag{20}$$

and

$$\frac{\mathcal{B}(\bar{B}^0 \to D^+\rho^-)}{\mathcal{B}(\bar{B}^0 \to D^{*+}\rho^-)} = 1.10 \pm 0.14 \pm 0.28. \tag{21}$$

The contribution in this ratio from the systematic error on the detection efficiency is reduced to 5% for these two cases. Both ratios of branching fractions are consistent with the expectation from HQET spin symmetry as well as the prediction from Blok and Shifman [63].

Mannel *et al.* [62] also observe that they can

obtain model dependent predictions for $\mathcal{B}(\bar{B}^0 \to D^+\rho^-)/\mathcal{B}(\bar{B}^0 \to D^+\pi^-)$ by using a combination of HQET, factorization, and data on $B \to D^*\ell\nu$ from CLEO and ARGUS. With three different parametrizations of the $B \to D$ form factor [64] this ratio is predicted to be 3.05, 2.52, or 2.61.

From the measurements of the branching ratios we obtain

$$\frac{\mathcal{B}(\bar{B}^0 \to D^+\rho^-)}{\mathcal{B}(\bar{B}^0 \to D^+\pi^-)} = 2.8 \pm 0.5 \pm 0.2. \tag{22}$$

The systematic errors from the D branching fractions and the tracking efficiency cancel in this ratio. Thus we find good agreement with the prediction from HQET combined with factorization.

XII. DIRECT AND INDIRECT EFFECTS OF THE COLOR SUPPRESSED AMPLITUDE

A. Introduction

In the QCD treatment described by Eqs. (1) and (2) it is difficult to take into account the effects of multiple soft gluon emission analytically. Instead, in the phenomenological BSW approach [34] two undetermined coefficients are assigned to the effective charged current $a_1(\mu)$ and the effective neutral current $a_2(\mu)$ parts of the B decay Hamiltonian. These coefficients were determined from a fit to a subset of the experimental data on charm decays. With these values the decay rates for a large number of nonleptonic decays can then be calculated using the factorization hypothesis, and model dependent hadron form factors. We can relate $a_1(\mu)$ and $a_2(\mu)$ to the QCD coefficients $c_1(\mu)$ and $c_2(\mu)$ by $a_1 = c_1 + \xi c_2$ and $a_2 = c_2 + \xi c_1$ where $\xi = 1/N_{color}$. The values $a_1(m_c^2) = 1.3$ and $a_2(m_c^2) = -0.55$ which give the best fit to the experimental data on charm decay correspond to $1/N_{color} \sim 0$ [8]. However, there is no rigorous theoretical justification for this choice of N_{color} [65].

In the decays of charmed mesons the effect of color suppression is obscured by the effects of final state interactions (FSI's) and soft gluon effects which enhance W exchange diagrams. For instance, Table XVIII gives ratios of several charmed meson decay modes with approximately equal phase space factors where the mode in the numerator is color suppressed while the mode in the denominator is an external spectator decay [66]. Clearly, these modes are not suppressed. However, the following decay appears to be suppressed:

$$\frac{\mathcal{B}(D^0 \to \bar{K}^0\rho^0)}{\mathcal{B}(D^0 \to K^-\rho^+)} = 0.08 \pm 0.04. \tag{23}$$

TABLE XVII. Ratios of B decay widths.

	Experiment	Factorization	RI model	BSW model
$\mathcal{B}(\bar{B}^0 \to D^{*+}\rho^-)/\mathcal{B}(\bar{B}^0 \to D^{*+}\pi^-)$	$2.9 \pm 0.5 \pm 0.5$	2.9 ± 0.05	$2.2 - 2.3$	2.8
$\mathcal{B}(\bar{B}^0 \to D^{*+}a_1^-)/\mathcal{B}(\bar{B}^0 \to D^{*+}\pi^-)$	$5.0 \pm 1.0 \pm 0.6$	3.4 ± 0.3	$2.0 - 2.1$	3.4

TABLE XVIII. Ratios of color suppressed to external spectator branching ratios.

$\mathcal{B}(D^0 \to \bar{K}^0\pi^0)/\mathcal{B}(D^0 \to K^-\pi^+)$	0.57 ± 0.13
$\mathcal{B}(D^0 \to \bar{K}^{*0}\pi^0)/\mathcal{B}(D^0 \to K^{*-}\pi^+)$	0.47 ± 0.23
$\mathcal{B}(D^0 \to \pi^0\pi^0)/\mathcal{B}(D^0 \to \pi^-\pi^+)$	0.77 ± 0.25
$\mathcal{B}(D_s^+ \to \bar{K}^{*0}K^+)/\mathcal{B}(D_s \to \phi\pi^+)$	0.95 ± 0.10
$\mathcal{B}(D_s^+ \to \bar{K}^0K^+)/\mathcal{B}(D_s \to \phi\pi^+)$	1.01 ± 0.16

In contrast with the charm sector where the mechanism of color suppression is obscured, one expects to find in *B* meson decays a simple and consistent pattern of color suppression. Partly, it is expected that color suppression is more effective at the *b* quark mass scale than the charm quark mass scale due to the evolution of the strong coupling constant α_s to smaller values. Using the BSW model and extrapolating from $q^2 = m_c^2$ to $q^2 = m_b^2$ using the values from charm decays gives the predictions $a_1(m_b^2) = 1.1$ and $a_2(m_b^2) = -0.24$ for *B* decays. Another approach using the factorization hypothesis, HQET, and model dependent form factors has been suggested by RI [32]. In this approach, a_1 and a_2 are determined from QCD (with $1/N_{color} = 1/3$) and color suppressed *B* decays are expected to occur at about 1/1000 the rate of unsuppressed decays. Observation of these decays at a much greater level would indicate the breakdown of the factorization hypothesis. In Sec. VIII we obtained upper limits for color-suppressed *B* decays with a D^0 or D^{*0} meson in the final state. In Table XIX these results are compared to prediction of the BSW and the RI model.

In contrast with charm decays, color suppression seems to be operative in hadronic decays of *B* mesons. The limits on the color-suppressed modes with $D^{0(*)}$ and neutral mesons are still above the level expected in the BSW model. However, the limit on $\bar{B}^0 \to D^0\pi^0$ disagrees with Terasaki's prediction [67] that $\mathcal{B}(\bar{B}^0 \to D^0\pi^0) \approx 1.8\,\mathcal{B}(\bar{B}^0 \to D^+\pi^-)$. To date, the only color-suppressed *B* meson decay modes which have been observed are final states which contain charmonium mesons, e.g., $B \to \psi K$ and $B \to \psi K^*$ [68].

TABLE XIX. Branching ratios of color suppressed *B* decays and comparisons with models.

Decay mode	UL (%)	BSW (%)	Γ (BSW)	RI model (%)
$\bar{B}^0 \to D^0\pi^0$	< 0.048	0.009	$0.201a_2^2$	$0.0013 - 0.0018$
$\bar{B}^0 \to D^0\rho^0$	< 0.055	0.006	$0.136a_2^2$	0.00044
$\bar{B}^0 \to D^0\eta$	< 0.068			
$\bar{B}^0 \to D^0\eta'$	< 0.086	0.00205	$0.03a_2^2$	
$\bar{B}^0 \to D^0\omega$	< 0.063	0.005	$0.06a_2^2$	
$\bar{B}^0 \to D^{*0}\pi^0$	< 0.097	0.009	$0.213a_2^2$	$0.0013 - 0.0018$
$\bar{B}^0 \to D^{*0}\rho^0$	< 0.117	0.010	$0.223a_2^2$	$0.0013 - 0.0018$
$\bar{B}^0 \to D^{*0}\eta$	< 0.069	0.0058	$0.07a_2^2$	
$\bar{B}^0 \to D^{*0}\eta'$	< 0.27	0.0033	$0.04a_2^2$	
$\bar{B}^0 \to D^{*0}\omega$	< 0.21	0.026	$0.31a_2^2$	

B. Determination of $|a_1|$, $|a_2|$, and the relative sign of (a_2/a_1)

In the BSW model [8,34], the branching fractions of the B^0 normalization modes are proportional to a_1^2 while the branching fractions of the $B \to \psi$ decay modes depend on a_2^2 (Table XX). A fit to the branching ratios that we have measured for the modes $\bar{B}^0 \to D^+\pi^-$, $D^+\rho^-$, $D^{*+}\pi^-$, and $D^{*+}\rho^-$ yields

$$|a_1| = 1.15 \pm 0.04 \pm 0.05 \pm 0.09, \qquad (24)$$

and a fit to the modes with ψ mesons in the final state gives

$$|a_2| = 0.26 \pm 0.01 \pm 0.01 \pm 0.02. \qquad (25)$$

The first systematic error on $|a_1|$ and $|a_2|$ includes the experimental uncertainties from the charm or charmonium branching ratios, tracking efficiency, background shapes, and the value of $|V_{cb}|$, but does not include the theoretical uncertainties. There is a second uncertainty due to the *B* meson production fractions and lifetimes. These are constrained by the value of $(f_+\tau_+/f_0\tau_0)$ determined from the CLEO II [69] measurement of $\mathcal{B}(B^- \to D^{*0}l^-\nu)/\mathcal{B}(\bar{B}^0 \to D^{*+}l^-\nu) = 1.20 \pm 0.20 \pm 0.19$.

TABLE XX. Branching ratios in terms of the BSW parameters a_1 and a_2. The coefficients are taken from Ref. [8].

Mode	B(%)
$\bar{B}^0 \to D^+\pi^-$	$0.264a_1^2$
$\bar{B}^0 \to D^+\rho^-$	$0.621a_1^2$
$\bar{B}^0 \to D^{*+}\pi^-$	$0.254a_1^2$
$\bar{B}^0 \to D^{*+}\rho^-$	$0.702a_1^2$
$B^- \to D^0\pi^-$	$0.265[a_1 + 1.230a_2\ (f_D/220)]^2$
$B^- \to D^0\rho^-$	$0.622[a_1 + 0.662a_2\ (f_D/220)]^2$
$B^- \to D^{*0}\pi^-$	$0.255[a_1 + 1.292a_2\ (f_{D^*}/220)]^2$
$B^- \to D^{*0}\rho^-$	$0.703[a_1^2 + 0.635a_2^2(f_{D^*}/220)^2 + 1.487a_1a_2\ (f_{D^*}/220)]$
$B^- \to \psi K^-$	$1.819a_2^2$
$B^- \to \psi K^{*-}$	$2.932a_2^2$
$\bar{B}^0 \to \psi\bar{K}^0$	$1.817a_2^2$
$\bar{B}^0 \to \psi\bar{K}^{*0}$	$2.927a_2^2$

TABLE XXI. Ratios of normalization modes to determine the sign of a_2/a_1. The magnitude of a_2/a_1 is the value in the BSW model which agrees with our result from $B \to \psi$ modes.

Ratio	$a_2/a_1 = -0.24$	$a_2/a_1 = 0.24$	CLEO II	RI model
R_1	0.50	1.68	$1.89 \pm 0.26 \pm 0.32$	$1.20 - 1.28$
R_2	0.71	1.34	$1.67 \pm 0.27 \pm 0.30$	$1.09 - 1.12$
R_3	0.48	1.72	$2.00 \pm 0.37 \pm 0.28$	$1.19 - 1.27$
R_4	0.41	1.85	$2.27 \pm 0.41 \pm 0.41$	$1.10 - 1.36$

The comparison of B^- and $\bar{B}^0$ modes can be used to distinguish between the two possible choices for the sign of a_2 relative to a_1. The BSW model, Ref. [8] predicts the ratios

$$R_1 = \frac{\mathcal{B}(B^- \to D^0\pi^-)}{\mathcal{B}(\bar{B}^0 \to D^+\pi^-)} = (1 + 1.23a_2/a_1)^2, \quad (26)$$

$$R_2 = \frac{\mathcal{B}(B^- \to D^0\rho^-)}{\mathcal{B}(\bar{B}^0 \to D^+\rho^-)} = (1 + 0.66a_2/a_1)^2. \quad (27)$$

The numerical factor that multiplies a_2/a_1 is proportional to the ratio of $B \to D^{(*)}$ to $B \to \pi(\rho)$ form factors as well as the ratio of the $\pi(\rho)$ meson to D meson decay constants. We assume $f_D = f_{D^*} = 220$ MeV [70]. Only the $B \to D^*$ form factor and the $\pi(\rho)$ meson decay constant have been measured experimentally.

Similarly, we define

$$R_3 = \frac{\mathcal{B}(B^- \to D^{*0}\pi^-)}{\mathcal{B}(\bar{B}^0 \to D^{*+}\pi^-)} = (1 + 1.29a_2/a_1)^2, \quad (28)$$

$$R_4 = \frac{\mathcal{B}(B^- \to D^{*0}\rho^-)}{\mathcal{B}(\bar{B}^0 \to D^{*+}\rho^-)} \approx (1 + 0.75a_2/a_1)^2. \quad (29)$$

Table XXI shows a comparison between the experimental results and the two allowed solutions in the BSW model. In these ratios, the systematic errors due to detection efficiency are reduced. In the ratios R_3 and R_4 the $D^0 \to K^-\pi^+$ branching ratio error does not contribute to the systematic error.

It is important to note that the determination of the sign of a_2/a_1 depends on assumptions about the relative production of B^+ and B^0 mesons at the $\Upsilon(4S)$ resonance, f_+ and f_0, as well as their lifetimes, τ_+ and τ_0. A least squares fit to the above ratios using the CLEO II value for $(f_+\tau_+/f_0\tau_0)$ [69] gives $a_2/a_1 = 0.23 \pm 0.04 \pm 0.04 \pm 0.10$ where we have ignored uncertainties in the theoretical predictions for R_1 through R_4. The second systematic error is due to the uncertainty in $(f_+\tau_+/f_0\tau_0)$. As this ratio increases, the value of a_2/a_1 decreases. The allowed range of $(f_+\tau_+/f_0\tau_0)$ excludes a negative value of a_2/a_1. Other uncertainties in the magnitude of f_D and the $B \to \pi$ form factor can change the magnitude of a_2/a_1 but not its sign. This result is consistent with the value of a_2 determined from the fit to the $B \to \psi$ decay modes. It disagrees with the theoretical extrapolation from data on charmed meson decay in the BSW model [71] which predicts a negative value for a_2/a_1.

XIII. CONCLUSIONS

We have presented new measurements of B branching ratios, resonant substructure, and masses. More accurate branching ratios are given for many modes. The modes $B \to D^*\rho^-$ and $B \to D^*a_1^-$ are clearly seen for the first time.

Using a subset of 702 B meson decays reconstructed in channels with good signal-to-background ratios we have made a precise measurement of the $\bar{B}^0 - B^-$ mass difference of $0.41 \pm 0.25 \pm 0.19$ MeV.

We have carried out an extensive series of tests of the factorization hypothesis including comparisons of rates for $D^{*+}h^-$ (where $h^- = \pi^-, \rho^-$, or a_1^-) with rates for $D^{*+}l^-\bar{\nu}$ at $q^2 = M_h^2$, as well as comparisons of the polarizations in $D^{*+}\rho^-$ with $D^{*+}\ell^-\bar{\nu}_\ell$. In all cases the factorization hypothesis is consistent with the data.

We have made improved measurements of branching ratios of two-body decays with a ψ, ψ', or χ_c meson in the final state. The decay $B \to \psi K^*$ is strongly polarized with $\Gamma_L/\Gamma = 0.80 \pm 0.08 \pm 0.05$. Therefore this mode will be useful for measuring CP violation.

A search for color suppressed decays with a charmed meson and light neutral hadron in the final state shows no positive evidence for such processes. The most stringent limit, $\mathcal{B}(\bar{B}^0 \to D^0\pi^0)/\mathcal{B}(\bar{B}^0 \to D^+\pi^-) < 0.09$, is still above the level where these color suppressed B decays are expected in most models.

The observation of $B \to \psi$ modes shows that color suppressed decays are present. Using only exclusive $B \to \psi$ decays we find a value of the BSW parameter $|a_2| = 0.26 \pm 0.01 \pm 0.01 \pm 0.02$. We also report a new value for the BSW parameter $|a_1| = 1.15 \pm 0.04 \pm 0.05 \pm 0.09$. Comparing B^+ and B^0 decays, we find $a_2/a_1 = 0.23 \pm 0.04 \pm 0.04 \pm 0.10$. We have shown that the sign of a_2/a_1 is positive, in contrast with what is found in charm decays.

APPENDIX

In this appendix, we provide the product of the *B* and charm branching fractions for the decay modes measured in this paper so that the results can be easily renormalized when the intermediate branching fractions for D^0, D^+, D^{*+}, D^{*0} and ψ, ψ', χ_{c1} mesons are known more precisely. The results are given in Tables XXII–XXVIII.

TABLE XXII. Product branching fractions (%) for $B^- \to D^0(n\pi)^-$ modes.

B^- mode	D mode	No. of events	ϵ	$\mathcal{B}[B^- \to D^0(n\pi)^-] \times \mathcal{B}(D^0 \to K^-[n\pi])$
	$K^-\pi^+$	76.3±9.1	0.433	0.0189 ± 0.0022 ± 0.0013
$D^0\pi^-$	$K^-\pi^+\pi^0$	134±15	0.193	0.0746 ± 0.0082 ± 0.0065
	$K^-\pi^+\pi^+\pi^-$	94± 11	0.222	0.0455 ± 0.0055 ± 0.0049
	$K^-\pi^+$	80 ± 9	0.155	0.0524 ± 0.0067 ± 0.0044
$D^0\rho^-$	$K^-\pi^+\pi^0$	42 ± 9	0.036	0.1254 ± 0.0282 ± 0.0150
	$K^-\pi^+\pi^+\pi^-$	90.4±12.1	0.079	0.1223 ± 0.0164 ± 0.0142

TABLE XXIII. Product branching fractions (%) for $\bar{B}^0 \to D^+(n\pi)^-$ modes.

$\bar{B}^0$ mode	D mode	No. of events	ϵ	$\mathcal{B}[\bar{B}^0 \to D^+(n\pi)^-]$ $\times \mathcal{B}(D^+ \to K^-\pi^+\pi^+)$
$D^+\pi^-$	$K^-\pi^+\pi^+$	80.6±9.8	0.32	0.0265 ± 0.0032 ± 0.0023
$D^+\rho^-$	$K^-\pi^+\pi^+$	78.9±10.7	0.12	0.0704 ± 0.0096 ± 0.0070

TABLE XXIV. Product branching fractions (%) for $B^- \to D^{*0}(n\pi)$ modes.

B^- mode	D^0 mode	No. of events	ϵ	$\mathcal{B}[B^- \to D^{*0}(n\pi)^-]$ $\times \mathcal{B}(D^{*0} \to D^0\pi^0) \times \mathcal{B}(D^0 \to K^-[n\pi])$
	$K^-\pi^+$	13.3±3.8	0.16	0.0090 ± 0.0026 ± 0.0009
$D^{*0}\pi^-$	$K^-\pi^+\pi^0$	37.7±6.9	0.08	0.0488 ± 0.0089 ± 0.0063
	$K^-\pi^+\pi^+\pi^-$	20.0±4.9	0.08	0.0267 ± 0.0065 ± 0.0033
	$K^-\pi^+$	25.7±5.4	0.064	0.0432 ± 0.0090 ± 0.0058
$D^{*0}\rho^-$	$K^-\pi^+\pi^0$	43.8±7.8	0.027	0.1722 ± 0.0305 ± 0.0300
	$K^-\pi^+\pi^+\pi^-$	16.9±4.6	0.030	0.0608 ± 0.0176 ± 0.0095
	$K^-\pi^+$	5.5±2.9	0.048	0.0124 ± 0.0065 ± 0.0020
$D^{*0}\pi^-\pi^-\pi^{+a}$	$K^-\pi^+\pi^0$	27.7±7.2	0.022	0.1316 ± 0.0343 ± 0.0237
	$K^-\pi^+\pi^+\pi^-$	15.0±4.5	0.025	0.0632 ± 0.0187 ± 0.0118

[a]The three pion mass is required to be between 1.0 GeV and 1.6 GeV, consistent with an a_1 meson. (If this channel is dominated by a_1^-, the branching ratio for $D^{*0}a_1^-$ is twice that for $D^{*0}\pi^-\pi^-\pi^+$.)

TABLE XXV. Product branching fractions (%) for $\bar{B}^0 \to D^{*+}(n\pi)^-$ modes.

$\bar{B}^0$ mode	D^0 mode	No. of events	ϵ^a	$\mathcal{B}[\bar{B}^0 \to D^{*+}(n\pi)^-]$ $\times \mathcal{B}(D^{*+} \to D^0\pi^+) \times \mathcal{B}(D^0 \to K^-[n\pi])$
	$K^-\pi^+$	19.4±4.5	0.35	0.0058 ± 0.0013 ± 0.0008
$D^{*+}\pi^-$	$K^-\pi^+\pi^0$	31.9±6.4	0.14	0.0243 ± 0.0049 ± 0.0035
	$K^-\pi^+\pi^+\pi^-$	20.5±5.2.	0.15	0.0146 ± 0.0033 ± 0.0025
	$K^-\pi^+$	21.9±5.2	0.12	0.0188 ± 0.0044 ± 0.0034
$D^{*+}\rho^-$	$K^-\pi^+\pi^0$	39.8±7.2	0.048	0.0892 ± 0.0162 ± 0.0177
	$K^-\pi^+\pi^+\pi^-$	14.6±4.6	0.054	0.0286 ± 0.0091 ± 0.0059
	$K^-\pi^+$	13.5±3.9	0.096	0.0151 ± 0.0044 ± 0.0024
$D^{*+}\pi^-\pi^-\pi^{+a}$	$K^-\pi^+\pi^0$	21.7±5.9	0.043	0.0545 ± 0.0147 ± 0.0091
	$K^-\pi^+\pi^+\pi^-$	13.9±4.4	0.042	0.0348 ± 0.0101 ± 0.0069

[a]The three pion mass is required to be between 1.0 GeV and 1.6 GeV consistent with an a_1 meson. (If this channel is dominated by a_1^-, the branching ratio for $D^{*+}a_1^-$ is twice that for $D^{*+}\pi^-\pi^-\pi^+$.)

TABLE XXVI. Product branching fractions for $B \to \psi$ modes and 90% confidence level upper limits (%).

B mode	No. of events	ϵ	$\mathcal{B}(B \to \psi K^{(*)})$ $\times \mathcal{B}(\psi \to l^+ l^-)$ [a]
$B^- \to \psi K^-$	58.7 ± 7.9	0.47	$0.0131 \pm 0.0017 \pm 0.0011$
$B^0 \to \psi K^0$	10.0 ± 3.2	0.34	$0.0088 \pm 0.0028 \pm 0.0009$
$B^0 \to \psi K^{*0}$	29.0 ± 5.4	0.23	$0.0200 \pm 0.0037 \pm 0.0021$
$B^- \to \psi K^{*-}$	12.6 ± 3.6		$0.0210 \pm 0.0061 \pm 0.0026$

[a]The product branching fraction has been corrected for the K^0, K^*, or K^0_S branching ratios but not for the ψ branching fractions.

TABLE XXVII. Product branching fractions for $B \to \psi'$ modes and 90% confidence level upper limits (%).

B mode	$\mathcal{B}(B \to \psi' K^{(*)}) \times \mathcal{B}(\psi')$ [a]
$B^- \to \psi' K^- \psi' \to l^+ l^-$	$0.0011 \pm 0.0006 \pm 0.0001$
$B^- \to \psi' K^-, \psi' \to \psi \pi^+ \pi^-$	$0.0173 \pm 0.0100 \pm 0.0023$
$B^0 \to \psi' K^0, \psi' \to l^+ l^-$	< 0.0025
$B^0 \to \psi' K^0, \psi' \to \psi \pi^+ \pi^-$	< 0.0200
$B^0 \to \psi' K^{*0}, \psi' \to l^+ l^-$	< 0.0051
$B^0 \to \psi' K^{*0}, \psi' \to \psi \pi^+ \pi^-$	< 0.0210
$B^- \to \psi' K^{*-}, \psi' \to l^+ l^-$	< 0.0065
$B^- \to \psi' K^{*-}, \psi' \to \psi \pi^+ \pi^-$	< 0.0600

[a]The product branching fraction has been corrected for the K^0, K^* or K^0_S branching ratios but not for the ψ' and ψ branching fractions. We give $\mathcal{B}(B \to \psi' K^{(*)}) \times \mathcal{B}(\psi' \to l^+ l^-)$ or $\mathcal{B}(B \to \psi' K^{(*)}) \times \mathcal{B}(\psi' \to \psi \pi^+ \pi^-) \times \mathcal{B}(\psi \to l^+ l^-)$.

TABLE XXVIII. Product branching fractions for $B \to \chi_{c1}$ modes and 90% confidence level upper limits (%).

B mode	No. of events	ϵ	$\mathcal{B}(B \to \chi_{c1} K^{(*)}) \times \mathcal{B}(\chi_{c1})$ [a]
$B^- \to \chi_{c1} K^-$	6 ± 2.4	0.20	$0.0031 \pm 0.0013 \pm 0.0003$
$B^0 \to \chi_{c1} K^0$	1 ± 1	0.14	< 0.0087
$B^0 \to \chi_{c1} K^{*0}$	1.2 ± 1.5	0.13	< 0.0066
$B^- \to \chi_{c1} K^{*-}$	0		< 0.0066

[a]For the modes with χ_{c1} mesons, we report the product $\mathcal{B}(B \to [\chi_{c1}]K^{(*)}) \times \mathcal{B}(\psi \to l^+ l^-) \times \chi_{c1} \to \gamma \psi$ branching fraction in the product. The product branching fraction has been corrected for the K^0, K^*, or K^0_S branching ratios but not for the ψ branching fractions.

[1] CLEO Collaboration, S. Behrends *et al.*, Phys. Rev. Lett. **50**, 881 (1983).

[2] CLEO Collaboration, M. S. Alam *et al.*, Phys. Rev. D **36**, 1289 (1987).

[3] CLEO Collaboration, D. Bortoletto *et al.*, Phys. Rev. D **45**, 21 (1992).

[4] ARGUS Collaboration, H. Albrecht *et al.*, Phys. Lett. B **185**, 218 (1987).

[5] ARGUS Collaboration, H. Albrecht *et al.*, Phys. Lett. B **215**, 424 (1988).

[6] ARGUS Collaboration, H. Albrecht *et al.*, Z. Phys. C **48**, 543 (1990).

[7] We make the approximation that V_{ud}, $V_{cs} \approx 1$.

[8] M. Neubert, V. Riekert, Q. P. Xu, and B. Stech, in *Heavy Flavours*, edited by A. J. Buras and H. Lindner (World Scientific, Singapore, 1992).

[9] J. Bjorken, in *Developments in High-Energy Physics*, Proceedings of the Conference, Crete, Greece, 1988, edited by E. G. Floratos and A. Verganelakis [Nucl. Phys. B (Proc. Suppl.) **11**, 325 (1989)].

[10] Y. Kubota *et al.*, Nucl. Instrum. Methods A **320**, 66 (1992); the crystal performance is described by R. Morrison *et al.*, Phys. Rev. Lett. **67**, 1696 (1991).

[11] Particle Data Group, K. Hikasa *et al.*, Phys. Rev. D **45**,

S1 (1992).

[12] CLEO Collaboration, D. Akerib *et al.*, Phys. Rev. Lett. **71**, 3070 (1993).

[13] The systematic uncertainty from the track reconstruction in $D^0 \to K^-\pi^+$ is common to this paper and to Ref. [12], and is only included in the systematic error on the *B* branching fraction. To avoid counting this systematic error twice, we use the value of $\mathcal{B}(D^0 \to K^-\pi^+) = (3.91 \pm 0.08 \pm 0.07)\%$ which does not include the tracking systematic error.

[14] Mark III Collaboration, J. Adler *et al.*, Phys. Rev. Lett. **60**, 89 (1988).

[15] CLEO Collaboration, F. Butler *et al.*, Phys. Rev. Lett. **69**, 2041 (1992).

[16] CLEO Collaboration, D. Bortoletto *et al.*, Phys. Rev. Lett. **69**, 2046 (1992).

[17] Mark III Collaboration, D. Coffman *et al.*, Phys. Rev. D **68**, 282 (1992).

[18] This requirement has an efficiency of 86% while reducing the background by a factor of 2.

[19] G. Fox and S. Wolfram, Phys. Rev. Lett. **23**, 1581 (1978).

[20] G. Hanson *et al.*, Phys. Rev. Lett. **35**, 1609 (1975); S. L. Wu and G. Zobernig, Z. Phys. C **2**, 107 (1979).

[21] The resolution in beam-constrained mass has a weak dependence on the decay channel. It varies between 2.6 MeV and 3.3 MeV.

[22] The lowest fraction is for the mode $\bar{B}^0 \to D^{*+}\rho^-$ while the highest fraction is for the mode $B^- \to D^0\pi^-$.

[23] For the case of $B^- \to D^0\rho^-$, $D^0 \to K^-\pi^+\pi^0$, we use only half of the helicity angle distribution used for the other modes ($\cos\Theta_\rho > 0.4$ instead of $|\cos\Theta_\rho| > 0.4$).

[24] The results of the analysis using only the forward hemisphere ($\cos\theta_\rho > 0.4$) are $\mathcal{B}(\bar{B}^0 \to D^0\rho^-) = 1.29 \pm 0.14 \pm 0.11$ and $\mathcal{B}(B^- \to D^+\rho^-) = 0.97 \pm 0.16 \pm 0.14$.

[25] We consider two models: nonresonant $B \to D\pi^-\pi^0$ and $B \to D^{**}(2460)\pi^-$. Both give very similar $\pi^-\pi^0$ mass spectra and comparable limits on the non-ρ contamination in the signal region.

[26] Also note that the corrected distribution is symmetric, indicating that the efficiency correction is reasonable (37.0 ± 5.5 entries in the forward hemisphere and 35.7 ± 5.4 entries in the backward hemisphere).

[27] J. D. Richman, California Institute of Technology Report No. CALT-68-1231, 1984 (unpublished).

[28] The corrected distribution for $\bar{B}^0 \to D^{*+}\rho^-$ is symmetric, indicating that the efficiency correction is reasonable (45.6 ± 6.7 entries in the forward hemisphere of D^{*+} helicity angle and 39.3 ± 6.3 entries in the backward hemisphere of D^{*+} helicity angle).

[29] CLEO Collaboration, S. Henderson *et al.*, Phys. Rev. D **45**, 2212 (1992).

[30] ARGUS Collaboration, H. Albrecht *et al.*, Phys. Lett. B **249**, 359 (1990); H. Albrecht *et al.*, Z. Phys. C **57**, 553 (1993).

[31] P. Colangelo, G. Nardulli, and N. Paver, Phys. Lett. B **303**, 152, 1993.

[32] C. Reader and N. Isgur, Phys. Rev. D **47**, 1007 (1993). The authors emphasize that their results for color suppressed decay have large theoretical uncertainties and are order of magnitude estimates rather than predictions.

[33] I. Dunietz *et al.*, Phys. Rev. D **43**, 2193 (1991).

[34] M. Bauer, B. Stech, and M. Wirbel, Z. Phys. C **29**, 637 (1985); **34**, 103 (1987); **42**, 671 (1989).

[35] G. Kramer and W. F. Palmer, Phys. Lett. B **279**, 181

(1992).

[36] These modes are also accessible via the *W*-exchange graph but this is expected to be small in *B* decay due to helicity suppression.

[37] The requirement that the colors match gives a factor of $1/3$ in the amplitude. Moreover, the *W* couples to the $d\bar{d}$ part of the π^0 wave function so there is an additional factor of $1/\sqrt{2}$ in the amplitude. This is also true for the ρ^0 and the ω mesons. The numerical factor is different for the case of the η/η' system.

[38] I. Dunietz and A. Snyder, Phys. Rev. D **43**, 1593 (1991). The D^0 meson, however, must decay to a *CP* eigenstate, e.g., $B \to D^0\pi^0$, $D^0 \to K^-K^+$ could be used.

[39] We use the PDG values for the η, η', and ω branching ratios [11].

[40] In the mode $\bar{B}^0 \to D^0\omega$, $\omega \to \pi^-\pi^+\pi^0$, we require that Θ_N, the angle between the normal to the ω decay plane and the D^0 direction calculated in the D^0 rest frame, satisfy $|\sin\Theta_N| > 0.6$.

[41] In Ref. [11], p. III.38.

[42] CLEO Collaboration, D. Bortoletto *et al.*, Phys. Rev. D **37**, 1719 (1988).

[43] A. S. Artamov *et al.*, Phys. Lett. **137B**, 272 (1984).

[44] The background shape is allowed to vary from being flat all the way to the kinematic limit, to having the functional form $f(x) = c_1 x \sqrt{(1 - x^2)} e^{c_2(1-x^2)}$, where $x = M_B/E_{\text{beam}}$.

[45] C. P. Singh *et al.*, Phys. Rev. D **24**, 788 (1981); L.-H. Chan, Phys. Rev. Lett. **51**, 253 (1983); K. P. Tiwari *et al.*, Phys. Rev. D **51**, 643 (1985); D. Y. Kim and S. N. Sinha, Ann. Phys. (N.Y.) **42**, 47 (1985).

[46] J. L. Goity and W. S. Hou, Phys. Lett. B **282**, 243 (1992); R. F. Lebed, Phys. Rev. D **47**, 1134 (1993).

[47] S. Stone, in *Heavy Flavours* [8].

[48] M. J. Dugan and B. Grinstein, Phys. Lett. B **255**, 583 (1991), references therein.

[49] N. Isgur and M. B. Wise, Phys. Lett. **32B**, 113 (1989); **37B**, 527 (1990).

[50] The error is due to the uncertainty in the scale at which to evaluate the Wilson coefficient.

[51] D. Bortoletto and S. Stone, Phys. Rev. Lett. **65**, 2951 (1990). It should be understood that the above relation is exact for the case when h^- is a vector meson. When h^- is a pseudoscalar meson only the longitudinal part of the semileptonic width enters into the determination of the left-hand state. For the case of $h = \pi^-$ discussed here, the correction for this effect is small.

[52] X. Y. Pham and X. C. Vu, Phys. Rev. D **46**, 261 (1992).

[53] The value $f_\rho = 196$ MeV derived from τ decays is determined using the narrow width approximation, i.e., by assuming the ρ resonance is a δ function.

[54] Since the form factor for $B \to D^*\ell\nu$ is slowly varying, the width of the ρ^- meson does not significantly modify the result.

[55] The value of c_1 is the Wilson coefficient evaluated at the *b* quark mass scale. The value of f_ρ is from $e^+e^- \to \rho^0$ data as determined by Pham and Vu. The value of V_{ud} is taken from J. Rosner, in *B decays*, edited by S. Stone (World Scientific, Singapore, 1992).

[56] The q^2 spectrum has been corrected for the new values of the CLEO II D^* and D branching ratios [15,12].

[57] J. Korner and G. Goldstein, Phys. Lett. **89B**, 105 (1979).

[58] Peter Lepage (private communication).

[59] J. L. Rosner, Phys. Rev. D **42**, 3732 (1990).

[60] M. Neubert, Phys. Lett. B **264**, 455 (1991).

[61] G. Kramer, T. Mannel, and W. F. Palmer, Z. Phys. C **55**, 497, 1992.

[62] T. Mannel *et al.*, Phys. Lett. B **259**, 359(1991). Similar observations have been made by a large number of other authors.

[63] B. Blok and M. Shifman, Nucl. Phys. **B389**, 534 (1993).

[64] Three parametrizations of the Isgur-Wise function $\xi(vv')$ are considered: (a) $\xi(vv') = 1 + 1/4a(v - v')^2(v + v')^2$ with $a = 0.54 \pm 0.01$, (b) $\xi(vv') = 1/[1 - (v - v')^2/w_0^2]$ with $w_0 = 1.12 \pm 0.17$, due to Rosner [59], and (c) $\xi(vv') = \exp[b(v - v')^2]$ with $b = 0.91 \pm 0.03$. All of these parametrizations are constrained by fitting to the average of the CLEO 1.5 and ARGUS data on $d\Gamma/dQ^2(B \rightarrow D^*\ell\nu)$.

[65] M. A. Shifman, Nucl. Phys. **B388**, 346 (1992).

[66] The branching ratios with the exception of that for the $D^0 \rightarrow \pi^0\pi^0$ decay mode are taken from the PDG (Ref. [11]). The $D^0 \rightarrow \pi^0\pi^0$ branching ratio is described by CLEO Collaboration, B. Ong *et al.*, Phys. Rev. Lett. **71**, 1973 (1993).

[67] K. Terasaki, Phys. Rev. D **47**, 5177 (1993).

[68] The branching ratio for the modes $B \rightarrow \psi K$ and $B \rightarrow \psi K^*$ can be accommodated by the value $\xi \sim 0$ while $\xi \sim 1/3$ gives a branching ratio that is about a factor of 4 too low (see Ref. [65]).

[69] CLEO Collboration, D. Akerib *et al.*, in the EPS Conference, Marseille, 1993 (unpublished).

[70] J. L. Rosner, in *Testing the Standard Model*, Proceedings of the Theoretical Advanced Study Institute in Elementary Particle Physics, edited by M. Cvetic and P. Langacker (World Scientific, Singapore, 1991).

[71] In the fits of Ref. [8], the CLEO 1.5 data favor a positive sign while the ARGUS data prefer a negative sign. From a global fit to data from both experiments, they find two solutions either $a_1 = 1.10 \pm 0.08$ and $a_2 = 0.20 \pm 0.02$ or $a_1 = 1.14 \pm 0.07$ and $a_2 = -0.17 \pm 0.02$.